Pergamon

Int. J. Solids Structures Vol. 33, No. 6, pp. 811–833, 1996

0020-7683/96 $9.50 + .00

0020-7683(95)00080-1

THE PROPAGATION OF SPHERICAL WAVES IN RATE-SENSITIVE ELASTIC-PLASTIC MATERIALS

PETER A. FOTIU and FRANZ ZIEGLER
Institut für Allgemeine Mechanik, Technical University of Vienna, A-1040 Vienna, Austria

(*Received* 13 *September* 1994; *in revised form* 25 *March* 1995)

Abstract—An integral equation method for the analysis of elastic-plastic wave propagation is presented. The elastic-plastic solution is thereby found as the superposition of the corresponding elastic result with waves produced by dynamically induced plastic strains. The solutions are represented in the form of integrals with elastodynamic Green's functions as integration kernels. The spherically symmetric problem of a dynamically loaded spherical cavity is considered and the corresponding Green's functions for this geometry are derived in closed form. Time convolution is carried out analytically over a prescribed time step and the spatial integration is performed by Gaussian quadrature. If the wave travels within each time step just the distance of one spatial element the evaluation of the integrals leads to a tridiagonal system of algebraic equations. Numerical results are compared to some known analytical solutions, proving the accuracy of the method. Computations are carried out for rate sensitive power law hardening–thermal softening materials.

1. INTRODUCTION

The problem of elastic-plastic wave propagation has received interest from many researchers. In particular, on the subject of spherical waves in isotropic solids important analytical work has been contributed by Hunter (1957), Chadwick and Morland (1969), Morland (1969), Chadwick (1970), and comparisons with numerical solutions by the finite difference method were presented by Mok (1968) and Milne *et al.* (1988). A detailed account of the subject as well as an extensive list of references is given by Hopkins (1960). All these studies consider the propagation of spherical waves from a dynamically expanding cavity, assuming rate independent ideal elastic-plastic material behavior or linear work-hardening. The mathematical approach in these papers focuses on the propagation of the elastic and the plastic shock fronts. The governing equations of the elastic as well as the plastic domain are formally derived in analytic form, but depend on the extension and propagation of the elastic–plastic interface. The analysis of Morland (1969) shows that in the loading range the plastic front propagates at a constant speed c_p for linear strain-hardening, provided that the pressure p at the cavity wall is applied as a step load and has an amplitude larger than the critical value $p_{cr} = \sigma_0 (1-\nu)/(1-2\nu)$, where σ_0 is the initial yield stress and ν is Poisson's ratio. If $p > p_{cr}$, the interface is a surface of discontinuity, and an analytic solution can be found for simple cases [e.g. Chadwick and Morland (1969) for linear work hardening]. These analytic results, however, are valid only as long as there is a stress discontinuity at the interface. Numerical computations show that these discontinuities decay rapidly and, consequently, the analytic results derived by Chadwick and Morland (1969) are limited to the early stages of the propagation of an elastic-plastic shock wave.

For $p \leqslant p_{cr}$ or continuous loading, the elastic–plastic interface carries no discontinuity and the interface velocity is always smaller than c_p. Then, an analytic result can be obtained only for the inverse problem, where the interface velocity is prescribed and the time varying cavity pressure is found accordingly (Hunter, 1957).

In this kind of analysis the solution is obtained from differential equations, which directly depend on the inelastic constitutive equations. The specific form of these constitutive relations determines whether an analytic solution exists or not. In addition to the previously discussed limitations any analytic results are valid only in the loading range, i.e. they break down if unloading occurs anywhere in the solid.

In this paper we develop a mathematical framework of wave propagation based on dynamic Green's functions. The elastic-plastic solution is thereby found by superposition of altogether *elastic* trains of waves, produced by the applied load as well as by the dynamically induced plastic strains. The resulting integral equations are integrated numerically with the constraint that the dynamic plastic strains satisfy the constitutive equations. The latter are used here merely as side conditions, which leaves the main analysis open to *any* type of constitutive behavior. There is also no need for a separate consideration of loading and unloading waves, because this is directly controlled by the determination of the plastic strain from the loading/unloading conditions in the constitutive law. This strategy allows the evaluation of stresses, displacements and deformation rates along the wave fronts and in the wake as well, and may be used to obtain a picture of the remaining state of selfstress in the material after a shock loading of the cavity walls. Along the same lines, material behavior other than elastoplasticity may also be treated. For example, waves in elastic layered media can be modeled, representing different elastic properties by equivalent eigenstrains as in Eshelby's method (Eshelby, 1957; Mura, 1987; Nemat-Nasser and Hori, 1993). Density differences, however, have to be treated as additional fictitious body forces (Mura, 1987; p. 459f.). In that context it is also possible to treat micromechanical problems of plasticity and/or damage. Then, those equivalent eigenstrains are found as averaged quantities from a micromechanical analysis of a representative volume element. For example, Güldenpfennig and Clifton (1980), in an attempt to study plastic waves in thin walled tubes, calculated the macroscopic plastic strains of a polycrystalline aggregate from crystallographic slip systems by the selfconsistent method.

In the first part of the paper we identify the necessary dynamic Green's functions from the dynamic Betti–Rayleigh reciprocal theorem. Later, these influence functions are specified for spherical symmetry, and a detailed outline of the numerical integration procedure is given. We use a rate-dependent elastic-plastic material law with power law strain hardening, that is sufficiently general to describe a variety of metallic materials. The formulation of the constitutive equation is such that rate-independent plasticity is included as a special case. Moreover, temperature effects due to plastic dissipation are taken into account. Because of the slow propagation of heat when compared to the wave velocity, only adiabatic heating will be considered. Numerous examples are used to demonstrate the efficiency of the method and to show several interesting effects in elastic-plastic wave propagation. Comparisons with some known analytic solutions underline the accuracy of the numerical procedure, even in the neighborhood of the plastic shock front.

2. DYNAMIC GREEN'S FUNCTIONS

The concept of dynamic Green's functions is derived from the dynamic Betti–Rayleigh reciprocity theorem (Eringen and Suhubi, 1975; p. 368), which reads for a body with volume V and surface S,

$$\int_V [\tilde{\mathbf{b}}(\mathbf{x})*\mathbf{u}(\mathbf{x})](t)\,\mathrm{d}V+\int_S [\tilde{\mathbf{t}}(\mathbf{x})*\mathbf{u}(\mathbf{x})](t)\,\mathrm{d}S+\rho\int_V (\dot{\tilde{\mathbf{u}}}(\mathbf{x},0)\cdot\mathbf{u}(\mathbf{x},t)+\tilde{\mathbf{u}}(\mathbf{x},0)\cdot\dot{\mathbf{u}}(\mathbf{x},t))\,\mathrm{d}V=$$

$$\int_V [\tilde{\mathbf{u}}(\mathbf{x})*\mathbf{b}(\mathbf{x})](t)\,\mathrm{d}V+\int_S [\tilde{\mathbf{u}}(\mathbf{x})*\mathbf{t}(\mathbf{x})](t)\,\mathrm{d}S+\rho\int_V (\dot{\tilde{\mathbf{u}}}(\mathbf{x},t)\cdot\mathbf{u}(\mathbf{x},0)+\tilde{\mathbf{u}}(\mathbf{x},t)\cdot\dot{\mathbf{u}}(\mathbf{x},0))\,\mathrm{d}V, \quad (1)$$

where $(\mathbf{u},\mathbf{b},\mathbf{t})$ and $(\tilde{\mathbf{u}},\tilde{\mathbf{b}},\tilde{\mathbf{t}})$ are two distinct sets of variables, denoting the vectors of displacement, body force and surface traction, respectively. The mass density is designated by ρ, a superposed dot indicates a time-derivative, and $[\cdot * \cdot]$ is the convolution, defined by

$$[\tilde{\mathbf{b}}(\mathbf{x})*\mathbf{u}(\mathbf{x})](t)=\int_0^t \tilde{\mathbf{b}}(\mathbf{x},t-\tau)\cdot\mathbf{u}(\mathbf{x},\tau)\,\mathrm{d}\tau. \quad (2)$$

We assume $\tilde{\mathbf{b}}$ to be a singular body force.

$$\tilde{\mathbf{b}} = \delta(t-\tau)\delta(\mathbf{x}-\mathbf{x}')\mathbf{e}, \tag{3}$$

where $\mathbf{e}$ is a unit vector and δ denotes the Dirac-delta function. The dimension of the delta function is determined by the dimension of its argument. Thus, $\delta(\mathbf{x}-\mathbf{x}')$ is a three-dimensional delta function, while $\delta(t-\tau)$ is one-dimensional. With eqn (3), we obtain from (1)

$$u_i(\mathbf{x},t) = \int_V [\tilde{u}_{i,j}(\mathbf{x}',\mathbf{x})*b_j(\mathbf{x}')](t)\,\mathrm{d}V(\mathbf{x}') + \int_S ([\tilde{u}_{i,j}(\mathbf{x}',\mathbf{x})*t_j(\mathbf{x}')](t)$$

$$-[\tilde{t}_{i,j}(\mathbf{x}',\mathbf{x})*u_j(\mathbf{x}')](t))\,\mathrm{d}S(\mathbf{x}') + \rho\int_V (\dot{\tilde{u}}_{i,j}(\mathbf{x}',\mathbf{x},t)u_j(\mathbf{x}',0) + \tilde{u}_{i,j}(\mathbf{x}',\mathbf{x},t)\dot{u}_j(\mathbf{x}',0))\,\mathrm{d}V(\mathbf{x}'), \tag{4}$$

where a primed index refers to $\mathbf{x}'$ and summation over repeated indices is understood. The Green's functions $\tilde{u}_{i,j}$ and $\tilde{t}_{i,j}$ are the displacement u_i and traction t_i in $\mathbf{x}'$, respectively, due to a unit force $\tilde{b}_i = \delta(t-\tau)\delta(\mathbf{x}-\mathbf{x}')e_i$ in $\mathbf{x}$. We assume linearized geometric relations for small strains, $\varepsilon_{ij} = (1/2)(u_{i,j}+u_{j,i})$. Note the symmetry of $\tilde{\mathbf{u}}$ with respect to the spatial coordinates, i.e. $\tilde{u}_{i,j}(\mathbf{x}',\mathbf{x},t) = \tilde{u}_{j,i}(\mathbf{x},\mathbf{x}',t)$.

Now consider the case where a body is loaded by a dynamic eigenstrain $\bar{\boldsymbol{\varepsilon}}(\mathbf{x},t)$. Introduction of the generalized Hooke's law $\boldsymbol{\sigma} = \mathbf{C}:(\boldsymbol{\varepsilon}-\bar{\boldsymbol{\varepsilon}})$ into the equilibrium conditions leads to

$$\nabla\cdot[\mathbf{C}:(\nabla\otimes\mathbf{u})] - \nabla\cdot(\mathbf{C}:\bar{\boldsymbol{\varepsilon}}) = \rho\ddot{\mathbf{u}}, \quad \mathbf{x}\in V, \tag{5a}$$

$$[\mathbf{C}:(\nabla\otimes\mathbf{u})]\cdot\mathbf{n} = (\mathbf{C}:\bar{\boldsymbol{\varepsilon}})\cdot\mathbf{n}, \mathbf{x}\in S^{\sigma}; \quad \mathbf{u} = 0, \mathbf{x}\in S^{u}, \tag{5b}$$

where ∇ is the gradient operator, $\mathbf{C}$ is the elasticity tensor and S^{σ}, S^{u} are those portions of the surface S, on which either the stresses or the displacements are prescribed. It follows from eqns (5) that the displacement in a solid with eigenstrains $\bar{\boldsymbol{\varepsilon}}(\mathbf{x},t)$ is the same as that produced by equivalent body forces $\bar{\mathbf{b}} = -\nabla\cdot(\mathbf{C}:\bar{\boldsymbol{\varepsilon}})$ and tractions $\bar{\mathbf{t}} = (\mathbf{C}:\bar{\boldsymbol{\varepsilon}})\cdot\mathbf{n}$. If we assume the body to be initially at rest ($\mathbf{u}(\mathbf{x},0) = \dot{\mathbf{u}}(\mathbf{x},0) = 0$) and introduce $\bar{\mathbf{b}}$ and $\bar{\mathbf{t}}$ for $\mathbf{b}$ and $\mathbf{t}$ in eqn (4), we find the displacement due to eigenstrains $\bar{\boldsymbol{\varepsilon}}$,

$$u_i(\mathbf{x},t) = \int_V [\tilde{\sigma}_{ij,k}(\mathbf{x}',\mathbf{x})*\bar{\varepsilon}_{jk}(\mathbf{x}')](t)\,\mathrm{d}V(\mathbf{x}'). \tag{6}$$

Physically, the function $\tilde{\sigma}_{ij,k}(\mathbf{x}',\mathbf{x},t-\tau)$ in eqn (6) represents the stress σ_{ij} in $\mathbf{x}'$ at time t due to a unit load $1\cdot e_k$ in $\mathbf{x}$ at time τ.

3. THE SPHERICALLY SYMMETRIC PROBLEM

3.1. *Loading by body forces*

We introduce spherical coordinates (r,ϑ,φ), and observe that under conditions of spherical symmetry the radial displacement $u_r = u$ is the only non-zero component. Furthermore, all variables depend only on the radius r and time t. Accordingly, eqn (4) simplifies to

$$u(r,t) = 4\pi\int_a^b [\tilde{u}(r',r)*b(r')](t)r'^2\,\mathrm{d}r' + 4\pi a^2[\tilde{u}(a,r)*p](t)$$

$$+ 4\pi\rho\int_a^b (\dot{\tilde{u}}(r',r,t)u(r',0) + \tilde{u}(r',r,t)\dot{u}(r',0))r'^2\,\mathrm{d}r', \tag{7}$$

where a is the cavity radius, $p(t)$ is the cavity pressure and $b(r)$ is a radially symmetric body force. Stresses and strains are obtained from the displacement (7) via the relations

$$\varepsilon_{rr} = u_{,r}, \quad \varepsilon_{\varphi\varphi} = \varepsilon_{\vartheta\vartheta} = u/r, \tag{8a}$$

$$\sigma_{rr} = (\lambda+2\mu)u_{,r} + 2\lambda u/r, \quad \sigma_{\varphi\varphi} = \sigma_{\vartheta\vartheta} = \lambda u_{,r} + 2(\lambda+\mu)u/r, \tag{8b}$$

where λ and μ are Lame's constants, and $()_{,r}$ denotes the derivative with respect to r.

The Green's function $\tilde{u}(r, r', t-\tau) = \tilde{u}(r', r, t-\tau)$ is found as the solution of the differential equation of the point-symmetric problem

$$\tilde{u}_{,rr} + \frac{2}{r}\left(\tilde{u}_{,r} - \frac{\tilde{u}}{r}\right) + (\lambda+2\mu)^{-1}\frac{\delta(t-\tau)\delta(r-r')}{4\pi r'^2} = \frac{\ddot{\tilde{u}}}{c_1^2}, \tag{9}$$

where $c_1 = (\lambda+2\mu/\rho)^{1/2}$ is the velocity of the dilatational wave and the forcing term in eqn (9) describes a singular radial load on a spherical surface of radius r', such that its volume integral is unity.

In the subsequent analysis we will use the following non-dimensional variables:

$$x = r/a, \quad x' = r'/a, \quad \bar{t} = c_1 t/a, \quad \bar{\tau} = c_1\tau/a, \tag{10a}$$

$$\zeta = \frac{2\mu}{\lambda+2\mu} = \frac{1-2\nu}{1-\nu}, \tag{10b}$$

$$\xi = \bar{t} - \bar{\tau} - \bar{x} + 1, \quad \bar{x} = x + x' - 1. \tag{10c}$$

With these definitions, the analytical solution of eqn (9) with traction-free boundary conditions at the cavity surface $[\sigma_{rr}(r=a)=0]$ has the form (details of the derivation are given in Appendix A),

$$\tilde{u}(x', x, \bar{t}-\bar{\tau}) = \tilde{u}^i(x', x, \bar{t}-\bar{\tau}) + \tilde{u}^r(x', x, \bar{t}-\bar{\tau}), \tag{11}$$

where

$$\tilde{u}^i(x', x, \bar{t}-\bar{\tau}) = \frac{c_1}{2\mu a^2}\frac{\zeta}{16\pi(xx')^2}(x^2+x'^2-(\bar{t}-\bar{\tau})^2)H(\bar{t}-d-\bar{\tau}) \tag{12a}$$

is the displacement of the incident wave, emanating from the source, and $\tilde{u}^r$, the wave reflected from the cavity, is found as

$$\tilde{u}^r(x', x, \bar{t}-\bar{\tau}) = \frac{c_1}{2\mu a^2}\frac{\zeta H(\xi)}{16\pi(xx')^2}\mathscr{W}(x', x, \bar{t}-\bar{\tau}), \tag{12b}$$

with

$$\mathscr{W}(x', x, \bar{t}-\bar{\tau}) = \xi^2 + 2(\bar{x}-1)\xi + 2xx' - 4\bar{x} + \frac{4\exp(-\zeta\xi)}{\omega}[(1+\zeta(\bar{x}-2xx'))\sin(\omega\xi) + \omega\bar{x}\cos(\omega\xi)]. \tag{13}$$

In eqns (12), (13) and further on, we use the abbreviations

$$d = |x - x'|, \tag{14a}$$

$$\omega = \sqrt{\zeta(2-\zeta)} = \frac{\sqrt{1-2\nu}}{1-\nu}, \tag{14b}$$

and $H(\cdot)$ denotes the Heaviside function.

If we set $x' = 1$ in eqn (11), we obtain the displacement field for a cavity, loaded by an impulsive unit pressure $p(t) = \delta(t)/4\pi a^2$ (Eringen and Suhubi, 1975; p. 481),

$$\tilde{u}(1, x, \bar{t}-\bar{\tau}) = \frac{c_1}{2\mu a^2}\frac{\zeta}{4\pi\omega x^2}\exp(-\zeta\xi)H(\xi)[(1-\zeta x)\sin(\omega\xi) + \omega x\cos(\omega\xi)], \tag{15}$$

with $\xi(x'=1) = \bar{t}-\bar{\tau}-x+1$. In the sequel, we will need also the time derivative of the Green's function $\tilde{u}$, which we denote by $\dot{\tilde{u}}$. Differentiating eqns (12a, b) and (15) gives

$$\dot{\tilde{u}}^{\mathrm{I}}(x', x, \bar{t}-\bar{\tau}) = -\frac{c_1^2}{2\mu a^3}\frac{\zeta}{8\pi(xx')^2}[(\bar{t}-\bar{\tau})H(\bar{t}-d-\bar{\tau}) - xx'\delta(\bar{t}-d-\bar{\tau})], \tag{16a}$$

$$\dot{\tilde{u}}^{\mathrm{r}}(x', x, \bar{t}-\bar{\tau}) = \frac{c_1^2}{2\mu a^3}\frac{\zeta}{8\pi(xx')^2}\left\{\left[\xi + \bar{x} - 1 - \frac{2\exp(-\zeta\xi)}{\omega}\right.\right.$$
$$\left.\left.\cdot[\zeta(1-2\zeta xx'+2\bar{x})\sin(\omega\xi) - \omega(1-2\zeta xx')\cos(\omega\xi)]\right]H(\xi) + xx'\delta(\xi)\right\}, \tag{16b}$$

$$\dot{\tilde{u}}(1, x, \bar{t}-\bar{\tau}) = -\frac{c_1^2}{2\mu a^3}\frac{\zeta}{4\pi\omega x^2}\{\exp(-\zeta\xi)[\zeta(1+2(1-\zeta)x)\sin(\omega\xi)$$
$$-\omega(1-2\zeta x)\cos(\omega\xi)]H(\xi) - \omega x\delta(\xi)\}. \tag{16c}$$

3.2. *Loading by eigenstrains*

The Green's functions $\tilde{\sigma}_{ijk}$ due to eigenstrains $\bar{\varepsilon}_{ij}$ are derived from $\tilde{u}$ according to relations (8b). With respect to later applications it becomes convenient to separate $\bar{\varepsilon}$ into a deviatoric and a hydrostatic part,

$$\bar{\varepsilon}_{ij} = \bar{\varepsilon}_{ij}^{\mathrm{d}} + \bar{\varepsilon}_{\mathrm{m}}\delta_{ij}, \quad (\cdot)_{\mathrm{m}} = (\cdot)_{ii}/3, \tag{17}$$

where the indices $(\cdot)^{\mathrm{d}}$ and $(\cdot)_{\mathrm{m}}$ identify the deviatoric and the mean component of a tensor, respectively. Under spherically symmetric conditions, the deviatoric components are related by, for example,

$$\bar{\varepsilon}_{rr}^{\mathrm{d}} = -2\bar{\varepsilon}_{\varphi\varphi}^{\mathrm{d}}, \tag{18}$$

and eqn (6) simplifies to

$$u(r, t) = 4\pi\int_a^\infty \{[\tilde{\sigma}(r', r) * \bar{\varepsilon}_{r'r'}^{\mathrm{d}}(r')](t) + 3[\tilde{\sigma}_{\mathrm{m}}(r', r) * \bar{\varepsilon}_{\mathrm{m}}(r')](t)\}r'^2\,\mathrm{d}r'. \tag{19}$$

The Green's functions $\tilde{\sigma}$ and $\tilde{\sigma}_{\mathrm{m}}$, appearing in eqn (19) are related to $\tilde{u}$ through

$$\tilde{\sigma} = \tilde{\sigma}_{r'r'} - \tilde{\sigma}_{\varphi'\varphi'} = 2\mu(\tilde{u}_{,r'} - \tilde{u}/r'), \tag{20a}$$

$$\tilde{\sigma}_{\mathrm{m}} = \tfrac{1}{3}(\tilde{\sigma}_{r'r'} + 2\tilde{\sigma}_{\varphi'\varphi'}) = 2\mu\frac{3-2\zeta}{3\zeta}(\tilde{u}_{,r'} + 2\tilde{u}/r'). \tag{20b}$$

With eqns (20), we obtain from eqns (12a, b) the following incident and reflected components

$$\tilde{\sigma}^{i}(x', x, \bar{t}-\bar{\tau}) = \frac{c_1}{a^3}\frac{\zeta}{16\pi x^2 x'^3}[(3(\bar{t}-\bar{\tau})^2 - 3x^2 - x'^2)H(\bar{t}-d-\bar{\tau}) + 2xx'^2\,\mathrm{sgn}(x-x')\delta(\bar{t}-d-\bar{\tau})], \quad (21a)$$

$$\tilde{\sigma}^{r}(x', x, \bar{t}-\bar{\tau}) = -\frac{c_1}{a^3}\frac{\zeta}{16\pi x^2 x'^3}\left\{\left[3\mathscr{H}(x', x, \bar{t}-\bar{\tau}) + 2x'^2 - \frac{8\zeta x'^2\exp(-\zeta\xi)}{\omega}\cdot[(1-\zeta x)\sin(\omega\xi) + \omega x\cos(\omega\xi)]\right]H(\xi) + 2xx'^2\delta(\xi)\right\}, \quad (21b)$$

$$\tilde{\sigma}^{i}_{\mathrm{m}}(x', x, \bar{t}-\bar{\tau}) = \frac{c_1}{a^3}\frac{3-2\zeta}{24\pi x^2 x'}[H(\bar{t}-d-\bar{\tau}) + x\,\mathrm{sgn}(x-x')\delta(\bar{t}-d-\bar{\tau})], \quad (22a)$$

$$\tilde{\sigma}^{r}_{\mathrm{m}}(x', x, \bar{t}-\bar{\tau}) = -\frac{c_1}{a^3}\frac{3-2\zeta}{24\pi x^2 x'}\left\{\left[1 - \frac{4\zeta\exp(-\zeta\xi)}{\omega}\cdot[(1-\zeta x)\sin(\omega\xi) + \omega x\cos(\omega\xi)]\right]H(\xi) + x\delta(\xi)\right\}, \quad (22b)$$

where the signum function is defined as $\mathrm{sgn}(x) = x/|x|$, $\forall\, x \neq 0$, $\mathrm{sgn}(0) = 0$.

Two types of eigenstrain have to be considered, namely the plastic strain $\boldsymbol{\varepsilon}^{\mathrm{p}}$, which is assumed deviatoric, and the thermal strain $\boldsymbol{\varepsilon}^{\mathrm{T}}$. The latter is considered to be of pure bulk type, i.e. $\varepsilon^{\mathrm{T}}_{ij} = \varepsilon^{\mathrm{T}}\delta_{ij} = \alpha(T-T_0)\delta_{ij}$, where α is the coefficient of linear thermal expansion, T is the temperature and T_0 is a reference temperature. Thus, we have

$$\bar{\varepsilon}^{\mathrm{d}}_{ij} = \varepsilon^{\mathrm{p}}_{ij}, \quad \bar{\varepsilon}_{\mathrm{m}} = \varepsilon^{\mathrm{T}} = \alpha(T-T_0). \quad (23)$$

While $\bar{\boldsymbol{\varepsilon}}(\mathbf{x}, t)$ is unknown in principle, the external load $p(t) = p_0 f(t)$ is a given function of time and the *elastic* wave due to $p(t)$ can be calculated independently. This solution, which is indicated by a superscript $(\cdot)^0$, reads

$$u^0(x, \bar{t}) = \frac{p_0}{2\mu}\frac{4\pi a^3}{c_1}[\tilde{u}(1, x)*f](\bar{t}), \quad (24a)$$

$$\dot{u}^0(x, \bar{t}) = \frac{p_0}{2\mu}\frac{4\pi a^3}{c_1}[\dot{\tilde{u}}(1, x)*f](\bar{t}), \quad (24b)$$

$$\varepsilon^{0\mathrm{d}}_{rr}(x, \bar{t}) = \frac{p_0}{2\mu}\frac{4\pi a^3}{c_1}[\tilde{e}(1, x)*f](\bar{t}). \quad (24c)$$

Relations (24) have to be complemented by the solution due to $\bar{\boldsymbol{\varepsilon}}(\mathbf{x}, t)$ (marked by a superscript $(\cdot)^*$), which has the form

$$u^*(x, \bar{t}) = \frac{4\pi a^4}{c_1}\int_1^{\infty}\{[\tilde{\sigma}(x', x)*\varepsilon^{\mathrm{p}}_{rr}(x')](\bar{t}) + 3[\tilde{\sigma}_{\mathrm{m}}(x', x)*\varepsilon^{\mathrm{T}}(x')](\bar{t})\}x'^2\,\mathrm{d}x' + 4\rho\pi a^3\int_1^{\infty}(\dot{\tilde{u}}(x', x, \bar{t})u^*(x', 0) + \tilde{u}(x', x, \bar{t})\dot{u}^*(x', 0))x'^2\,\mathrm{d}x', \quad (25a)$$

$$\dot{u}^*(x,\bar{t}) = \frac{4\pi a^4}{c_1}\int_1^x \{[\dot{\tilde{\sigma}}(x',x)*\dot{\varepsilon}^{\mathrm{p}}_{rr}(x')](\bar{t}) + 3[\dot{\tilde{\sigma}}_{\mathrm{m}}(x',x)*\dot{\varepsilon}^{\mathrm{T}}(x')](\bar{t})\}x'^2\,\mathrm{d}x'$$

$$+4\rho\pi a^3\int_1^x (\ddot{\tilde{u}}(x',x,\bar{t})u^*(x',0)+\dot{\tilde{u}}(x',x,\bar{t})\dot{u}^*(x',0))x'^2\,\mathrm{d}x', \quad (25b)$$

$$\varepsilon^{*\mathrm{d}}_{rr}(x,\bar{t}) = \frac{4\pi a^4}{c_1}\int_1^x \{[\dot{\tilde{s}}(x',x)*\dot{\varepsilon}^{\mathrm{p}}_{rr}(x')](\bar{t}) + 3[\dot{\tilde{s}}_{\mathrm{m}}(x',x)*\dot{\varepsilon}^{\mathrm{T}}(x')](\bar{t})\}x'^2\,\mathrm{d}x'$$

$$+4\rho\pi a^3\int_1^x (\dot{\tilde{e}}(x',x,\bar{t})u^*(x',0)+\tilde{e}(x',x,\bar{t})\dot{u}^*(x',0))x'^2\,\mathrm{d}x'. \quad (25c)$$

Consequently, the total result is the sum of the portions (24) and (25), $u = u^0 + u^*$, etc. The Green's functions $\dot{\tilde{\sigma}}$, $\dot{\tilde{\sigma}}_{\mathrm{m}}$, $\ddot{\tilde{u}}$, $\dot{\tilde{s}}$, $\dot{\tilde{s}}_{\mathrm{m}}$, $\dot{\tilde{e}}$, $\tilde{e}$ appearing in (25b, c) are found as derivatives of $\tilde{\sigma}$, $\tilde{\sigma}_{\mathrm{m}}$ and $\tilde{u}$, with respect to either r or t. The analytic expressions of these functions are given in Appendix B.

Finally, the stress components are derived from displacements u and deviatoric strains $\varepsilon^{\mathrm{d}}_{rr}$ via the relations

$$\sigma_{rr} = \frac{2\mu}{\zeta}\left(\frac{3}{2}\varepsilon^{\mathrm{d}}_{rr} - \zeta\varepsilon^{\mathrm{p}}_{rr} + (3-2\zeta)(u/r-\varepsilon^{\mathrm{T}})\right), \quad (26a)$$

$$\sigma_{\varphi\varphi} = \frac{2\mu}{\zeta}\left(\frac{3}{2}(1-\zeta)\varepsilon^{\mathrm{d}}_{rr} + \frac{\zeta}{2}\varepsilon^{\mathrm{p}}_{rr} + (3-2\zeta)(u/r-\varepsilon^{\mathrm{T}})\right). \quad (26b)$$

4. INCREMENTAL FORMULATION

Owing to the nonlinear dependence of $\dot{\varepsilon}^{\mathrm{p}}$ on the current state of the body the integral equations (25) have to be solved incrementally. We subdivide the radius into a sufficient number of line elements of equal non-dimensional length Δx and consider a finite time step $\Delta\bar{t} = \Delta x$, such that the wave front advances just past the distance between two neighboring points.

There are several strategies in solving wave propagation problems by integral equations. One possible way is to focus only on the location of sources, that is, external loadings or boundary conditions, which are not satisfied by the Green's functions. At each instant, all signals arriving at a selected location have to be summed up, i.e. the time convolutions have to be performed over the entire excitation history. This requires the storage of these histories of each source, but the spatial discretization is limited to the location of these sources. Such a procedure proves useful in computations of *elastic* wave propagation. An application of this strategy to plastic spherical waves has been devised by Ziegler *et al.* (1995).

An alternative method is to evaluate displacements and velocities at each instant throughout the (discretized) continuum, and use these as initial conditions for the next time step. In this case, the convolutions have to be performed only over *one* time step, and no storage of any excitation history is necessary. On the other hand, this method requires a discretization of the entire volume penetrated by the wave. In inelastic materials, however, such a discretization is unavoidable anyway, in order to satisfy the constitutive equations in each point. Hence, the latter method seems to be more appealing for *plastic* wave propagation problems and we will use it in the sequel.

Assume that we know the state at the beginning of a time step, $t = t_{\mathrm{a}}$, and we rewrite eqns (25) for the time increment $\Delta t = t_{\mathrm{b}} - t_{\mathrm{a}}$, where subscripts a and b denote quantities at the beginning and at the end of the time step, respectively. Taking, for example (25a), we find

$$u_b^*(x,\bar{t}_b) = \frac{4\pi a^4}{c_1}\int_{x-\Delta\bar{t}}^{x+\Delta\bar{t}}\int_0^{\Delta\bar{t}}\{\tilde{\sigma}(x',x,\Delta\bar{t}-\bar{\tau})\varepsilon_{rr}^{p}(x',\bar{\tau})+3\tilde{\sigma}_m(x',x,\Delta\bar{t}-\bar{\tau})\varepsilon^{T}(x',\bar{\tau})\}\,d\bar{\tau}x'^2\,dx'$$

$$+4\rho\pi a^3\int_{x-\Delta\bar{t}}^{x+\Delta\bar{t}}\{\dot{\tilde{u}}(x',x,\Delta\bar{t})u_a^*(x',\bar{t}_a)+\tilde{u}(x',x,\bar{t})\dot{u}_a^*(x',\bar{t}_a)\}x'^2\,dx', \quad (27)$$

and analogous expressions follow for (25b, c).

Note that within Δt a disturbance applied at t_a travels only a distance $\Delta r = c_1\Delta t$, and, hence, the space integration extends only over the interval $x-\Delta\bar{t} \leqslant x' \leqslant x+\Delta\bar{t}$. Moreover, at all discrete points except the first one at $x = 1$, only the *incident* components of the corresponding Green's functions have to be integrated, because within a timestep Δt a reflected wave can only arrive at a point located in the interval $1 \leqslant x < 1+\Delta\bar{t}$.

In the evaluation of integrals like (27), we use linear shape functions in time and space. Accordingly, each variable $a(x',\Delta\bar{t})$ within an element is represented by the sum

$$a(x'(\eta),\bar{t}) = \sum_{k=1}^{2} N^k(\eta)H(\bar{t}-\bar{t}_a)\left(a_a^k+\Delta a^k\frac{\bar{t}-\bar{t}_a}{\Delta t}\right), \quad (28)$$

where

$$x'(\eta) = \sum_{k=1}^{2} N^k(\eta)x'^k,$$

η is a local coordinate, $-1 \leqslant \eta \leqslant 1$, and a superscript k refers to the k-th nodal point in *local* numbering within a line element. The linear shape functions $N^k(\eta)$ are given by

$$N^1 = \frac{1-\eta}{2}, \quad N^2 = \frac{1+\eta}{2}. \quad (29)$$

The time integrals in eqn (27), etc., are performed analytically and the subsequent integration over x' is carried out numerically by Gaussian quadrature.

Elementwise numerical integration transforms integral equations like (27) into algebraic equations. We use vector notation, where column vectors are written in bold face and matrices are enclosed in brackets. The symbols of these vectors and matrices coincide with those of the corresponding Green's functions and state variables, respectively. In such a formulation (27) and the equivalent integrals for $\dot{u}_b^*$ and ε_{rrb}^{*d} read

$$\mathbf{u}_b^* = [\tilde{\boldsymbol{\sigma}}]^a\boldsymbol{\varepsilon}_a^p+[\tilde{\boldsymbol{\sigma}}]^\Delta\Delta\boldsymbol{\varepsilon}^p+[\tilde{\boldsymbol{\sigma}}_m]^a\boldsymbol{\varepsilon}_a^T+[\tilde{\boldsymbol{\sigma}}_m]^\Delta\Delta\boldsymbol{\varepsilon}^T+[\tilde{\mathbf{u}}]\mathbf{u}_a^*+[\tilde{\mathbf{u}}]\dot{\mathbf{u}}_a^*, \quad (30a)$$

$$\dot{\mathbf{u}}_b^* = [\dot{\tilde{\boldsymbol{\sigma}}}]^a\boldsymbol{\varepsilon}_a^p+[\dot{\tilde{\boldsymbol{\sigma}}}]^\Delta\Delta\boldsymbol{\varepsilon}^p+[\dot{\tilde{\boldsymbol{\sigma}}}_m]^a\boldsymbol{\varepsilon}_a^T+[\dot{\tilde{\boldsymbol{\sigma}}}_m]^\Delta\Delta\boldsymbol{\varepsilon}^T+[\ddot{\tilde{\mathbf{u}}}]\mathbf{u}_a^*+[\dot{\tilde{\mathbf{u}}}]\dot{\mathbf{u}}_a^*, \quad (30b)$$

$$\boldsymbol{\varepsilon}_b^{*d} = [\tilde{\mathbf{s}}]^a\boldsymbol{\varepsilon}_a^p+[\tilde{\mathbf{s}}]^\Delta\Delta\boldsymbol{\varepsilon}^p+[\tilde{\mathbf{s}}_m]^a\boldsymbol{\varepsilon}_a^T+[\tilde{\mathbf{s}}_m]^\Delta\Delta\boldsymbol{\varepsilon}^T+[\dot{\tilde{\mathbf{e}}}]\mathbf{u}_a^*+[\tilde{\mathbf{e}}]\dot{\mathbf{u}}_a^*, \quad (30c)$$

where it is understood that the vectors $\boldsymbol{\varepsilon}_b^{*d}$, $\boldsymbol{\varepsilon}_a^p$ and $\Delta\boldsymbol{\varepsilon}^p$ contain only rr-components.

From the time integration of eqn (28) it follows that there are contributions from the initial value a_a^k and from the increment Δa^k. Hence, each Green's function that is integrated over τ yields two matrices, indicated by the superscripts $[\cdot]^a$ and $[\cdot]^\Delta$. We will briefly demonstrate this by evaluating the first two terms on the right of (30a) which are associated to the variable ε_{rr}^p, from the integral equation (27). Using a linear time variation for ε_{rr}^p according to (28) and inserting (21a) for the Green's function $\tilde{\sigma}'$, we get

$$u_b^*(x,\bar{t}_b) = \frac{a_\zeta^c}{4x^2}\int_{x-\Delta\bar{t}}^{x+\Delta\bar{t}}\int_0^{\Delta\bar{t}}\frac{1}{x'}\{(3(\Delta\bar{t}-\bar{\tau})^2-3x^2-x'^2)H(\Delta\bar{t}-d-\bar{\tau})$$

$$+2xx'\,\mathrm{sgn}(x-x')\delta(\Delta\bar{t}-d-\bar{\tau})\}\left(\varepsilon_{r'r'}^{p}(x')+\frac{\Delta\varepsilon_{r'r'}^{p}(x')}{\Delta\bar{t}}\bar{\tau}\right)\mathrm{d}\bar{\tau}\,\mathrm{d}x'+\cdots$$

$$=\frac{a_\zeta^c}{4x^2}\int_{x-\Delta\bar{t}}^{x+\Delta\bar{t}}H(\Delta\bar{t}-d)\left\{\left[\frac{\Delta\bar{t}-d}{x'}(\Delta\bar{t}(\Delta\bar{t}+d)-2x(x+x'))\right.\right.$$

$$\left.+2xx'\,\mathrm{sgn}(x-x')\right]\varepsilon_{r'r'a}^{p}(x')+\left[\frac{\Delta\bar{t}-d}{4x'}(\Delta\bar{t}(\Delta\bar{t}+2d)-3x(x+2x')+x'^2)\right.$$

$$\left.\left.+2xx'\,\mathrm{sgn}(x-x')\right]\frac{\Delta\bar{t}-d}{\Delta\bar{t}}\Delta\varepsilon_{r'r'}^{p}(x')\right\}\mathrm{d}x'+\ldots. \tag{31}$$

where the contributions from ε^T and from the initial conditions have not been written down explicitly. The space integration of the right hand side of (31) is now carried out by Gaussian quadrature, using the linear shape functions (29) to approximate the variations of $\varepsilon_{r'r'a}^{p}(x')$ and $\Delta\varepsilon_{r'r'}^{p}(x')$ within the element. It becomes clear from (31) that integrations of the terms in the first bracket constitute the components of the matrix $[\tilde{\sigma}]^a$ while $[\tilde{\sigma}]^\Delta$ is obtained from those inside the second bracket.

While this kind of numerical integration follows those in many applications of the boundary element method (see, for example, Banerjee, 1994), some care has to be taken in evaluating integrals containing derivatives of delta functions. There are three different types of integrals involving a derivative of a delta function, each with a different argument, $\delta'(\Delta\bar{t}-d-\bar{\tau})$, $\delta'(\xi)$ and $\delta'(\Delta\bar{t}-d)$. The first two kinds appear, for example, in the Green's function $\tilde{s}^i$ and $\tilde{s}^r$, respectively (see Appendix B), and they are integrated over the *time* interval $\Delta\bar{t}$. Writing the corresponding terms of the Green's functions according to $g(x',x,\Delta\bar{t}-\bar{\tau})\ \delta'(\Delta\bar{t}-d-\bar{\tau})$ or $g(x',x,\xi)\ \delta'(\xi)$, where g is a continuous function of its arguments, the time integrals can be evaluated as

$$\int_0^{\Delta\bar{t}} g(x',x,\Delta\bar{t}-\bar{\tau})a(x',\bar{\tau})\delta'(\Delta\bar{t}-d-\bar{\tau})\,\mathrm{d}\bar{\tau}=\sum_{k=1}^{2}N^k(\eta)\left\{g_{,x'}(x'(\eta),x,d(\eta))\left(a_a^k+\Delta a^k\frac{\Delta\bar{t}-d(\eta)}{\Delta\bar{t}}\right)\right.$$

$$\left.+g(x'(\eta),x,d(\eta))\left(a_a^k\delta(\Delta\bar{t}-d(\eta))+\frac{\Delta a^k}{\Delta t}\right)\right\}, \tag{32a}$$

$$\int_0^{\Delta\bar{t}} g(x',x,\xi)a(x',\bar{\tau})\delta'(\xi)\,\mathrm{d}\bar{\tau}=\sum_{k=1}^{2}N^k(\eta)\left\{-g_{,\xi}(x'(\eta),x,0)\left(a_a^k+\Delta a^k\frac{\Delta\bar{t}-x-x'(\eta)+2}{\Delta\bar{t}}\right)\right.$$

$$\left.+g(x'(\eta),x,0)\left(a_a^k\delta(\Delta\bar{t}-x-x'(\eta)+2)+\frac{\Delta a^k}{\Delta\bar{t}}\right)\right\}, \tag{32b}$$

where, again $a(x',\bar{t})$ stands for any state variable, a_a^k is its value at the k-th discrete point in the element and $\Delta a^k = a_b^k - a_a^k$. The right-hand-sides of (32a, b) are now functions of x and the local coordinate η and the subsequent space integration over x' can be performed by Gaussian integration within the interval $-1\leqslant\eta\leqslant 1$.

The third kind of the derivative δ' appears in the evaluation of strains and velocities from initial conditions, for example in the Green's function $\tilde{e}(x',x,\bar{t})$ in (25c). In this case integration is performed over the *space* interval $x-\Delta\bar{t}\leqslant x'\leqslant x+\Delta\bar{t}$, giving

$$\int_{x-\Delta\bar{t}}^{x+\Delta\bar{t}} g(x', x, \Delta\bar{t}) u_a(x') \delta'(\Delta\bar{t} - d)\, dx'$$

$$= \begin{cases} g_{,x'}(x+\Delta\bar{t}, x, \Delta\bar{t}) u_a(x+\Delta\bar{t}) + g(x+\Delta\bar{t}, x, \Delta\bar{t}) u_{a,x'}(x+\Delta\bar{t}), & x' > x \\ -g_{,x'}(x-\Delta\bar{t}, x, \Delta\bar{t}) u_a(x-\Delta\bar{t}) - g(x-\Delta\bar{t}, x, \Delta\bar{t}) u_{a,x'}(x-\Delta\bar{t}), & x' < x \end{cases} \quad (33)$$

The last term in (33) requires the evaluation of $u_{a,r}$. In the subsequent numerical analysis we store only the kinematic variables u, $\dot{u}$ and ε^d_{rr}, and from these we evaluate $u_{a,r}$ as $u_{a,r} = (3/2)\varepsilon^d_{rra} + u_a/r$.

What remains now is to establish an incremental formulation of the elastic plastic constitutive equations, that delivers a relation between the unknown vectors $\Delta\boldsymbol{\varepsilon}^p$ and $\Delta\boldsymbol{\varepsilon}^T$ and the current state variables.

5. INELASTIC CONSTITUTIVE EQUATIONS AND THEIR NUMERICAL INTEGRATION

We assume rate dependent plasticity with combined isotropic and kinematic power law hardening and a J_2-flow condition. The constitutive framework is comprised in the following set of equations,

$$\dot{\boldsymbol{\varepsilon}}^p = \dot{\gamma}\boldsymbol{\mu}, \quad \boldsymbol{\mu} = \tfrac{3}{2}(\boldsymbol{\xi}^d/\xi), \quad \boldsymbol{\mu} : \boldsymbol{\mu} = \tfrac{3}{2}, \quad (34)$$

$$\dot{\gamma} = \sqrt{\tfrac{2}{3}\dot{\boldsymbol{\varepsilon}}^p : \dot{\boldsymbol{\varepsilon}}^p}, \quad \gamma = \int_0^t \dot{\gamma}\, dt \quad (35)$$

$$\boldsymbol{\xi}^d = \boldsymbol{\sigma}^d - \boldsymbol{\beta}, \quad \xi = \sqrt{\tfrac{3}{2}\boldsymbol{\xi}^d : \boldsymbol{\xi}^d}, \quad (36)$$

$$\dot{\boldsymbol{\beta}} = H'(\gamma, \dot{\gamma}, T)\dot{\boldsymbol{\varepsilon}}^p, \quad H' = \partial H/\partial\gamma, \quad H(\gamma, \dot{\gamma}, T) = \chi(\dot{\gamma}, T)\mathscr{H}_0\gamma^m, \quad (37)$$

$$f = \xi - g(\gamma, \dot{\gamma}, T) = 0, \quad (38)$$

$$g(\gamma, \dot{\gamma}, T) = \chi(\dot{\gamma}, T)(\sigma_0 + \mathscr{K}_0\gamma^n), \quad (39)$$

$$\chi(\dot{\gamma}, T) = (\dot{\gamma}/\dot{\varepsilon}_0)^n \exp(-\vartheta(T - T_0)). \quad (40)$$

Here, $\boldsymbol{\xi}^d$ is the stress difference between the Cauchy stress deviator $\boldsymbol{\sigma}^d$ and the back stress $\boldsymbol{\beta}$. Furthermore, $\dot{\gamma}$ denotes the effective plastic strain rate and γ is the accumulated plastic strain. By σ_0 we denote the initial yield stress, $\dot{\varepsilon}_0$ is a reference strain rate and $\mathscr{H}_0$, $\mathscr{K}_0$, m, n, ϑ are material constants. The function $\chi(\dot{\gamma}, T)$ in (37) and (39) describes rate dependence and thermal softening and appears as part of the isotropic hardening function $g(\gamma, \dot{\gamma}, T)$ as well as of the kinematic hardening function $H(\gamma, \dot{\gamma}, T)$. The function f constitutes the rate- and temperature-dependent yield condition. Rate-independent plasticity is achieved by setting $n = 0$, and isothermal plastic flow requires $\vartheta = 0$. For ideal elastic-plastic behavior we have to set also $\mathscr{H}_0 = \mathscr{K}_0 = 0$.

Adiabatic temperature changes due to plastic dissipation are governed by

$$\dot{T} = \frac{\dot{W}^p}{\rho c_v}, \quad (41)$$

where c_v is the specific heat per unit mass, and $\dot{W}^p$ is the plastic work rate. Equation (41) neglects heat conduction, which is reasonable in plastic wave propagation problems, since for most materials the propagation velocity of heat is negligibly small when compared to c_1.

A detailed outline of the numerical integration of eqns (34)–(41) by the generalized midpoint rule is given by Fotiu (1995) in a general setting, i.e. for arbitrary variations of the loading direction. In our problem, however, there is no change in the loading direction because of the spherical symmetry. Thus, $\boldsymbol{\mu}$ stays constant during continuous loading, and in unloading $\boldsymbol{\mu}$ merely changes its sign. Using $(34)_2$ and $(36)_1$, we may formally write

$$\boldsymbol{\mu}_b = \frac{3}{2g_b}(\boldsymbol{\xi}_a^d + \Delta\boldsymbol{\sigma}^d - \Delta\boldsymbol{\beta}), \tag{42}$$

and integrating $(37)_1$ according to the backward Euler method yields

$$\Delta\boldsymbol{\beta} = \boldsymbol{\mu}_b \int_{\gamma_a}^{\gamma_b} H'(\gamma, \dot{\gamma}, T)\, d\gamma \cong (H_b - H_a)\boldsymbol{\mu}_b. \tag{43}$$

with $\dot{\gamma}$ and T assumed to remain constant during the integration. Note that (43) is *exact* if H is independent of $\dot{\gamma}$ and T. Using $(34)_{1,2}$, (43) and the generalized Hooke's law $\Delta\boldsymbol{\sigma}^d = 2\mu(\Delta\boldsymbol{\varepsilon}^d - \Delta\boldsymbol{\varepsilon}^p)$, we are able to rewrite (42) as

$$(g_b + (3\mu + H_b^*)\Delta\gamma)\boldsymbol{\mu}_b = 3\mu(\boldsymbol{\varepsilon}_b^d - \boldsymbol{\varepsilon}_a^p - \boldsymbol{\beta}_a/2\mu). \tag{44}$$

From (44) we obtain the scalar equation

$$g_b + (3\mu + H_b^*)\Delta\gamma = 3\mu\Delta e, \tag{45}$$

where

$$\Delta e = \sqrt{\tfrac{2}{3}}(\boldsymbol{\varepsilon}_b^d - \boldsymbol{\varepsilon}_a^p - \boldsymbol{\beta}_a/2\mu) : (\boldsymbol{\varepsilon}_b^d - \boldsymbol{\varepsilon}_a^p - \boldsymbol{\beta}_a/2\mu) = |\varepsilon_{rrb}^d - \varepsilon_{rra}^p - \beta_{rra}/2\mu|, \tag{46}$$

$$H_b^* = \frac{3}{2}\frac{H_b - H_a}{\Delta\gamma}. \tag{47}$$

Relation (45) represents a nonlinear equation in the unknowns $\Delta\gamma$ and ΔT, provided $\boldsymbol{\varepsilon}_b^d$ and, hence, Δe are given. With $(37)_3$, (39) and (40) the functions g_b, H_b and χ_b at the end of the time step are given by

$$g_b = \chi_b(\sigma_0 + \mathscr{H}_0(\gamma_a + \Delta\gamma)^m), \tag{48a}$$

$$H_b = \chi_b \mathscr{H}_0(\gamma_a + \Delta\gamma)^m, \tag{48b}$$

$$\chi_b = \left(\frac{\Delta\gamma}{\dot{\varepsilon}_0 \Delta t}\right)^n \exp(-\vartheta(T_a + \Delta T - T_0)). \tag{48c}$$

Equation (45) has to be complemented by an incremental form of (41),

$$\Delta T = \frac{1}{\rho c_v}\int_{t_a}^{t_b} \dot{W}^p\, dt. \tag{49}$$

The proper form of $\dot{W}^p$ depends on the microstructural material properties, i.e. the amount of reversible energy stored during hardening. Here, we assume

$$\dot{W}^p = \boldsymbol{\sigma} : \dot{\boldsymbol{\varepsilon}}^p = \xi\dot{\gamma} + \boldsymbol{\beta} : \dot{\boldsymbol{\varepsilon}}^p. \tag{50}$$

Inserting (50) into (49) and carrying out the integration using relations (37)–(39), we obtain an approximation of the adiabatic temperature increment

$$\Delta T = \frac{1}{\rho c_v}\left[\int_{\gamma_a}^{\gamma_b} g\,\mathrm{d}\gamma + \int_{\gamma_a}^{\gamma_b} (\boldsymbol{\beta}_a + (H - H_a)\boldsymbol{\mu}) : \boldsymbol{\mu}\,\mathrm{d}\gamma\right]$$

$$\cong \frac{\chi_b}{\rho c_v}\left[(\sigma_0 - \tfrac{3}{2}\mathscr{H}_0\gamma_a^m)\Delta\gamma + \frac{\mathscr{H}_0 + (3/2)\mathscr{H}_0}{m+1}((\gamma_a + \Delta\gamma)^{m+1} - \gamma_a^m)\right] + \frac{\Delta\gamma\boldsymbol{\beta}_a : \boldsymbol{\mu}_b}{\rho c_v}. \quad (51)$$

Equations (45) and (51) are solved iteratively by a secant algorithm with initial guesses $\Delta\gamma^{(1)} = \Delta e - g_a/3\mu$ and $\Delta T^{(1)} = 0$ (more details about this numerical procedure can be found in Fotiu, 1995). With the solutions $\Delta\gamma$ and ΔT, the plastic and thermal strains are updated as

$$\varepsilon_{rrb}^p = \varepsilon_{rra}^p + \Delta\gamma\,\mathrm{sgn}(\mu_{rr}), \quad \varepsilon_b^T = \alpha(T_a + \Delta T - T_0). \quad (52)$$

6. GLOBAL EQUILIBRIUM ITERATIONS

Knowing the increments of ε_{rr}^p and ε^T, a new estimate of ε_{rr}^d is calculated from the global equations (30c) and (24c), and the same procedure is repeated until global equilibrium is obtained within a certain tolerance limit. We write

$$\boldsymbol{\varepsilon}_b^d = [\tilde{\mathbf{s}}]^\Delta \Delta\boldsymbol{\varepsilon}^p + [\tilde{\mathbf{s}}_m]^\Delta \Delta\boldsymbol{\varepsilon}^T + \mathbf{k}, \quad (53)$$

where

$$\mathbf{k} = \boldsymbol{\varepsilon}_b^{0d} + [\tilde{\mathbf{s}}]^a \boldsymbol{\varepsilon}_a^p + [\tilde{\mathbf{s}}_m]^a \boldsymbol{\varepsilon}_a^T + [\dot{\tilde{\mathbf{e}}}]\mathbf{u}_a^* + [\tilde{\mathbf{e}}]\dot{\mathbf{u}}_a^*, \quad (54)$$

contains all contributions, which stay constant during the iteration. If we assume $\boldsymbol{\varepsilon}_b^d$ as the global unknown, a standard Newton algorithm has the form

$$\boldsymbol{\varepsilon}_{b(n)}^d = \boldsymbol{\varepsilon}_{b(n-1)}^d - \mathbf{G}_{(n-1)}^{-1}\mathbf{r}_{(n-1)}, \quad (55)$$

with

$$\mathbf{r}_{(n)} = \boldsymbol{\varepsilon}_{b(n)}^d - [\tilde{\mathbf{s}}]^\Delta \Delta\boldsymbol{\varepsilon}^p(\boldsymbol{\varepsilon}_{b(n)}^d) - [\tilde{\mathbf{s}}_m]^\Delta \Delta\boldsymbol{\varepsilon}^T(\boldsymbol{\varepsilon}_{b(n)}^d) - \mathbf{k}, \quad (56)$$

$$\mathbf{G}_{(n)} = \mathbf{I} - [\tilde{\mathbf{s}}]^\Delta \left(\frac{\mathrm{d}\Delta\boldsymbol{\varepsilon}^p}{\mathrm{d}\boldsymbol{\varepsilon}_b^d}\right)_{(n)} - [\tilde{\mathbf{s}}_m]^\Delta \left(\frac{\mathrm{d}\Delta\boldsymbol{\varepsilon}^T}{\mathrm{d}\boldsymbol{\varepsilon}_b^d}\right)_{(n)}. \quad (57)$$

It must be emphasized that in the present method the numerical inversion of the gradient matrix $\mathbf{G}$ is rather inexpensive, because of the banded nature of the matrices $[\tilde{\mathbf{s}}]^\Delta$ and $[\tilde{\mathbf{s}}_m]^\Delta$. While static integral equation methods usually deal with fully populated Green's matrices, the use of dynamic Green's functions leads here to banded matrices which can be inverted by special subroutines. The bandwith depends on the ratio $\Delta\bar{t}/\Delta x$. In the numerical computations of Section 7 we will use $\Delta\bar{t} = \Delta x$, and in that case $[\tilde{\mathbf{s}}]^\Delta$ and $[\tilde{\mathbf{s}}_m]^\Delta$ as well as all other matrices become tridiagonal.

In order to retain the quadratic convergence rate of the Newton method, it is necessary to calculate the *local* derivatives $\mathrm{d}\Delta\boldsymbol{\varepsilon}^p/\mathrm{d}\boldsymbol{\varepsilon}_b^d$ and $\mathrm{d}\Delta\boldsymbol{\varepsilon}^T/\mathrm{d}\boldsymbol{\varepsilon}_b^d$. In integral equation methods these derivatives are the equivalent to the elastoplastic consistent tangent operator in finite element methods (Simo and Taylor, 1985, 1986). The first gradient is found by differentiating (45),

$$\frac{\mathrm{d}\Delta\varepsilon^{\mathrm{p}}_{rr}}{\mathrm{d}\varepsilon^{\mathrm{d}}_{rr\mathrm{b}}} = \frac{\mathrm{d}\Delta\varepsilon^{\mathrm{p}}_{rr}}{\mathrm{d}\Delta\gamma}\frac{\mathrm{d}\Delta\gamma}{\mathrm{d}\varepsilon^{\mathrm{d}}_{rr\mathrm{b}}} = \mu_{rr}\frac{3\mu}{3\mu+g'_{\mathrm{b}}+(3/2)H'_{\mathrm{b}}}\operatorname{sgn}(\mu_{rr}) = \frac{3\mu}{3\mu+g'_{\mathrm{b}}+(3/2)H'_{\mathrm{b}}}, \tag{58}$$

where $g'_{\mathrm{b}} = \mathrm{d}g_{\mathrm{b}}/\mathrm{d}\Delta\gamma$, $H'_{\mathrm{b}} = \mathrm{d}H_{\mathrm{b}}/\mathrm{d}\Delta\gamma$, and $|\mu_{rr}| = 1$ has been used. While (58) is exact if the functions g and H are temperature-independent, they are only approximations in a temperature-dependent calculation. However, the influence of temperature variations on the plastic strain increment is usually small and we expect the simple formula (58) still to be a sufficiently accurate expression for the derivative $\mathrm{d}\Delta\boldsymbol{\varepsilon}^{\mathrm{p}}/\mathrm{d}\boldsymbol{\varepsilon}^{\mathrm{d}}_{\mathrm{b}}$. The variation of the thermal strain increment is derived from differentiating (51)

$$\frac{\mathrm{d}\Delta\varepsilon^{\mathrm{T}}}{\mathrm{d}\varepsilon^{\mathrm{d}}_{rr\mathrm{b}}} = \alpha\frac{\mathrm{d}\Delta T}{\mathrm{d}\Delta\gamma}\frac{\mathrm{d}\Delta\gamma}{\mathrm{d}\varepsilon^{\mathrm{d}}_{rr\mathrm{b}}} = \alpha\left[\frac{n}{\Delta\gamma}\Delta T + \frac{1}{\rho c_{\mathrm{v}}}(g_{\mathrm{b}}+H_{\mathrm{b}}-H_{\mathrm{a}}+\boldsymbol{\beta}_{\mathrm{a}}:\boldsymbol{\mu})\right]\frac{3\mu}{3\mu+g'_{\mathrm{b}}+(3/2)H'_{\mathrm{b}}}\operatorname{sgn}(\mu_{rr}), \tag{59}$$

where again, variations of g and H with temperature are neglected.

Iterations are stopped if

$$\frac{|\boldsymbol{\varepsilon}^{\mathrm{d}}_{\mathrm{b}(n)} - \boldsymbol{\varepsilon}^{\mathrm{d}}_{\mathrm{b}(n-1)}|}{|\boldsymbol{\varepsilon}^{\mathrm{d}}_{\mathrm{b}(n)}|} < tol, \tag{60}$$

where tol is the tolerance limit of the error. Having found $\boldsymbol{\varepsilon}^{\mathrm{d}}_{\mathrm{b}}$ and the plastic and thermal strains from (52), displacements and velocities at $t = t_{\mathrm{b}}$ are calculated from (24a, b) and (30a, b) and the stress components are then obtained from (26a, b).

7. ILLUSTRATIVE EXAMPLES

7.1. *Ideal elastic-plastic material*

At first the accuracy of the numerical results is tested in comparison to analytic solutions, derived by Chadwick and Morland (1969). Rate-independent ideal elastic-plastic material behavior is assumed and a step load $p(t) = p_0 H(t)$ is applied at the cavity wall. If $p_0/\sigma_0 > 1/\zeta$, which is termed supercritical loading by Chadwick and Morland (1969), a stress and velocity jump will occur at the elastic–plastic interface, that advances at a constant speed $c_{\mathrm{p}} = \sqrt{(1+\nu)/3(1-\nu)}\,c_1$. As long as the stress jump does not vanish and there is no unloading behind the discontinuity, an analytic solution can be given. In Figs 1–3 this analytic result is shown together with numerical calculations for $\nu = 0.315$ and

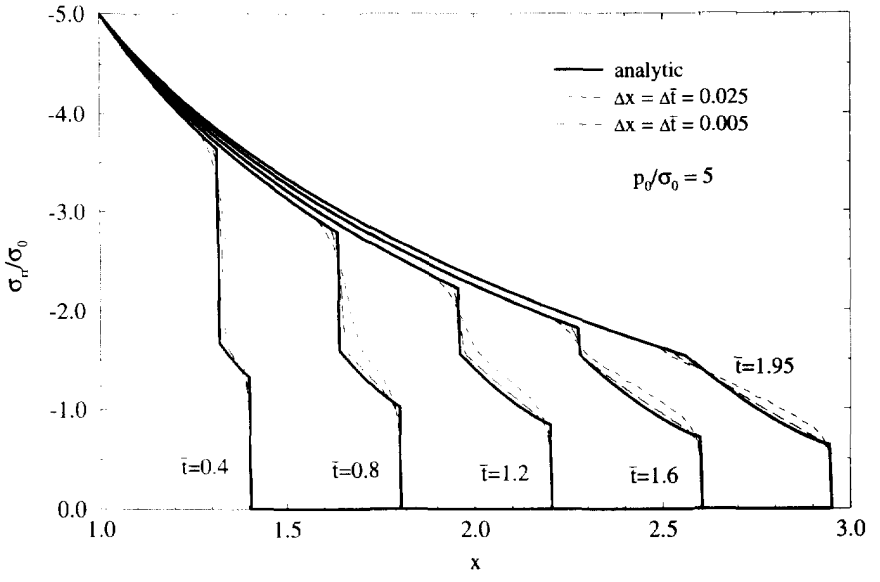

Fig. 1. Radial stress distribution in an ideal elastic-plastic material for a step load $p_0/\sigma_0 = 5$. Analytic results of Chadwick and Morland (1969) and numerical solution for step lengths $\Delta x = 0.025$, $\Delta x = 0.005$.

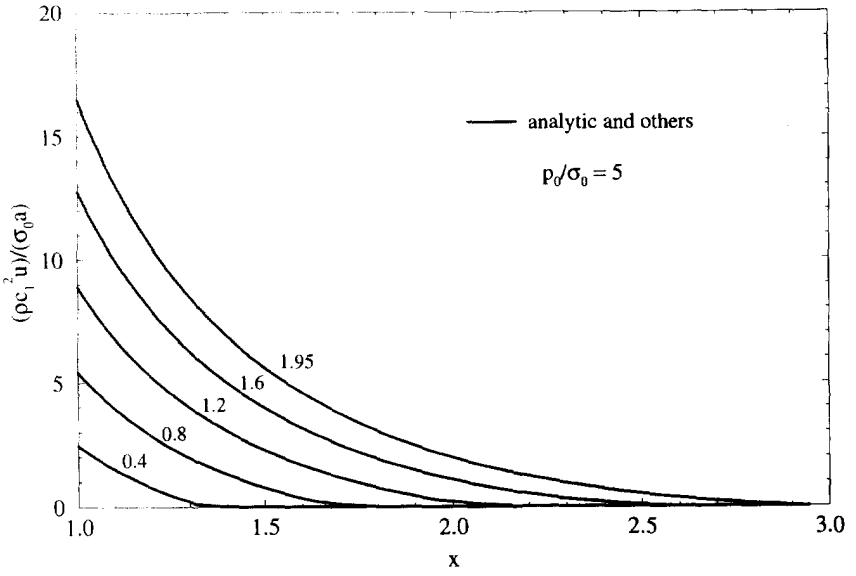

Fig. 2. Displacements in an ideal elastic-plastic material for a step load $p_0/\sigma_0 = 5$. There is no visible difference between the analytical and the numerical results.

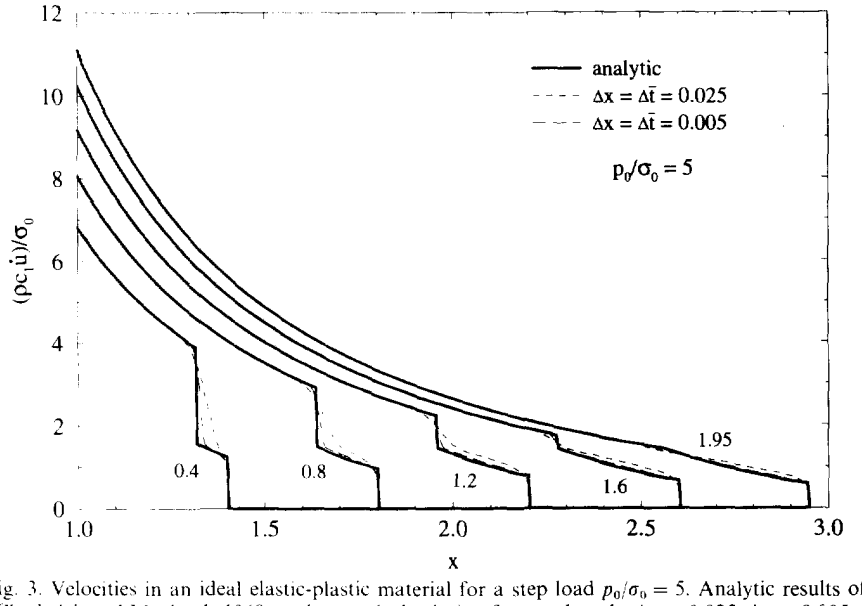

Fig. 3. Velocities in an ideal elastic-plastic material for a step load $p_0/\sigma_0 = 5$. Analytic results of Chadwick and Morland (1969) and numerical solution for step lengths $\Delta x = 0.025$, $\Delta x = 0.005$.

$p_0/\sigma_0 = 5$. Figure 1 demonstrates that the present method yields highly accurate results for the stresses, except at the jump at the elastic–plastic interface and along the elastic precursor. Depending on the grid size, corners of the stress profile are more or less rounded. The fine discretization $\Delta x = 0.005$ already gives a close agreement with the exact result along the entire stress range. The analytical solution of Chadwick and Morland (1969) is valid only until $\bar{t} = 1.95$, where the plastic shock front vanishes.

The non-dimensional displacements $(\rho c_1^2/\sigma_0)(u/a)$ are given in Fig. 2, where the results for both step lengths are practically indistinguishable from the analytic solution. A picture similar to the radial stress is obtained for the non-dimensional velocity $(\rho c_1^2/\sigma_0)(\dot{u}/c_1)$. Again, excellent agreement with the exact solution is found for $\Delta x = 0.005$ (Fig. 3).

In the previous example no unloading occurred in the plotted range. To study the effects of unloading and reloading we apply two rectangular pulses, each of a duration of

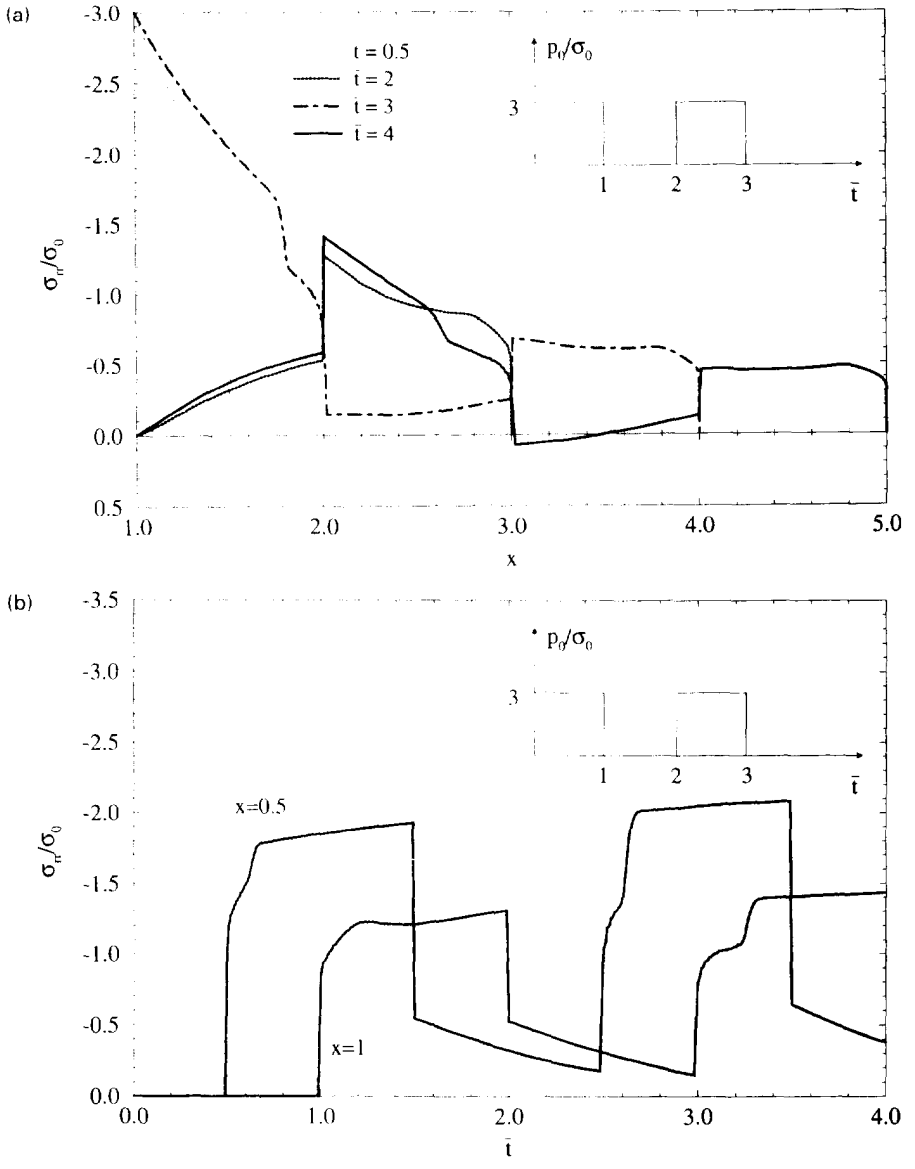

Fig. 4. Radial stress distribution in an ideal elastic-plastic material for a loading by two successive pressure pulses $p_0/\sigma_0 = 3$. (a) Spatial distribution; (b) time variation at $x = 0.5, 1$.

$\bar{t} = 1$, with a resting period of the same length inbetween (Fig. 4a). The intensity of the pulses is $p_0/\sigma_0 = 3$. Here, as well as in all remaining examples in this paper, we use a Poisson's ratio of $\nu = 0.3$.

Plots of the radial stress vs x and $\bar{t}$ are shown in Fig. 4(a, b) for a step length $\Delta x = \Delta\bar{t} = 0.01$. At initial loading the discontinuity at the elastic–plastic interface vanishes at a time $\bar{t} = 0.76$, and at $\bar{t} = 0.5$ the stress jump is clearly visible. After the end of the first pressure pulse an unloading wave develops, which propagates with a speed $c_1 > c_p$. The second pulse again causes plastic loading, creating a plastic shock front with an elastic precursor. However, this time the discontinuity at the elastic-plastic interface lasts substantially longer. It is well developed at a time $\bar{t} = 3$ and still clearly visible at $\bar{t} = 4$, that is twice the pulse duration after the second loading. This can also be observed from Fig. 4b, which shows the time variation of σ_r at the two locations $x = 0.5$ and $x = 1$. In plastic loading the stresses reach a nearly constant plateau, before the drop due to the unloading wave. A step-like dent in the rising slope indicates an elastic precursor. While at $x = 0.5$

both pulses exhibit an elastic and a plastic front, only the second pulse in $x = 1$ shows such a step-like profile. Phenomena like internal reflections of elastic unloading waves at plastic shock fronts as described by Kolsky (1963; p. 170 ff.) in the uniaxial case (see also Irschik and Ziegler, 1990), occur in principle also for spherical waves, but owing to numerical dispersion, these effects may not be easily detected in a numerical analysis.

7.2. *Rate-independent power-law hardening material*

We assume combined isotropic and kinematic strain hardening as described in Section 5. To study the Bauschinger effect in an otherwise equivalently hardening material we derive the isotropic and kinematic hardening moduli $\mathscr{K}_0$ and $\mathscr{H}_0$ from a total hardening modulus K_0 as

$$\mathscr{K}_0 = bK_0, \quad \mathscr{H}_0 = \tfrac{2}{3}(1-b)K_0, \tag{61}$$

where b, $0 \leqslant b \leqslant 1$, may be termed as the degree of isotropic hardening, since for $b = 1$ we obtain pure isotropic hardening and $b = 0$ represents pure kinematic hardening. In order to study the material response for different values of b, we have to ensure reverse plastic loading. Hence, we assume the following loading function: $p(t) = p_0$, $0 \leqslant \bar{t} \leqslant 1$, $p(t) = -p_0$, $1 \leqslant \bar{t} \leqslant 2$, $p(t) = 0$, $\bar{t} \geqslant 2$. Strain hardening is described by the parameters $K_0/\sigma_0 = 1$ and $m = 0.3$. Results of the radial and circumferential stress components are displayed in Fig. 5(a–c). Application of the first pressure pulse again leads to the development of an elastic precursor and an elastic plastic interface, though, due to nonlinear hardening, there is no longer an exact jump in the stresses and the velocity. In Fig. 5 we compare solutions for pure isotropic hardening ($b = 1$, bold lines) with those of pure kinematic hardening ($b = 0$, thin lines). During the initial phase of loading the stresses coincide for both types of hardening, owing to the assumption of the same total hardening modulus K_0. Differences appear after reverse loading, where the Bauschinger effect leads to reverse plastifications at a lower stress level, and the stress profile for $b = 0$ slightly lags behind that for isotropic hardening. Owing to the prescribed boundary conditions $\sigma_{rr}(x = 1) = -p_0(t)$ differences are more pronounced in the circumferential stress component $\sigma_{\varphi\varphi}$ (Fig. 5b, c).

7.3. *Rate-dependent power-law hardening and thermal softening material*

Next, we study the effect of the rate-dependence of the yield stress. The cavity is loaded by a rectangular pulse of intensity $p_0/\sigma_0 = 6$ and duration $\bar{t} = 1$. The viscoplastic material behavior is modelled by the following parameters, which are typical for metals: $m = 0.2$, $K_0/\sigma_0 = 1$, $\dot{\varepsilon}_0 a/c_1 = 10^{-8}$, $b = 1$. The results for two different exponents of the rate sensitivity $n = 0.01$, 0.02 are compared with the rate independent solution $n = 0$. Figure 6 shows the radial distribution of the effective stress σ at different times. A rate sensitivity of $n = 0.02$ elevates the effective stress at the cavity surface approximately by a factor of 4/3. As the wave progresses the differences in the stress peaks become smaller, and, eventually at $\bar{t} = 4$, they are roughly of the same magnitude. At this time, $\sigma < \sigma_0$ everywhere, and the wave travels elastically.

Finally, we will consider also thermal influences. We assume the same rate-sensitive material as above with $n = 0.02$ and $\rho c_v T_0/\sigma_0 = 0.005$, $\vartheta T_0 = 1$, $\alpha T_0 = 3.5 \times 10^{-3}$. Again, the cavity is loaded by a rectangular pulse, but with a duration of $\bar{t} = 2$. The effect of thermal softening becomes visible in Fig. 7, where effective stresses are plotted over time. Significant softening appears only close to the cavity wall where most of the plastic dissipation and, consequently, the maximum temperature rise take place (Fig. 8). At $x = 1$, there is an initial overshoot in the stress, which drops immediately to an equilibrium value. This is typical for viscoplasticity (Bodner and Aboudi, 1983), where due to rapid loading the material initially behaves elastically and relaxes according to its degree of viscosity, described by the constants n and $\dot{\varepsilon}_0$. The extension of the (adiabatic) temperature field indicates also the extension of the plastic zone. At $\bar{t} = 3$, the domain $x < 2$ already undergoes unloading and at $\bar{t} = 4$ there is only a marginal further extension of the plastic zone up to

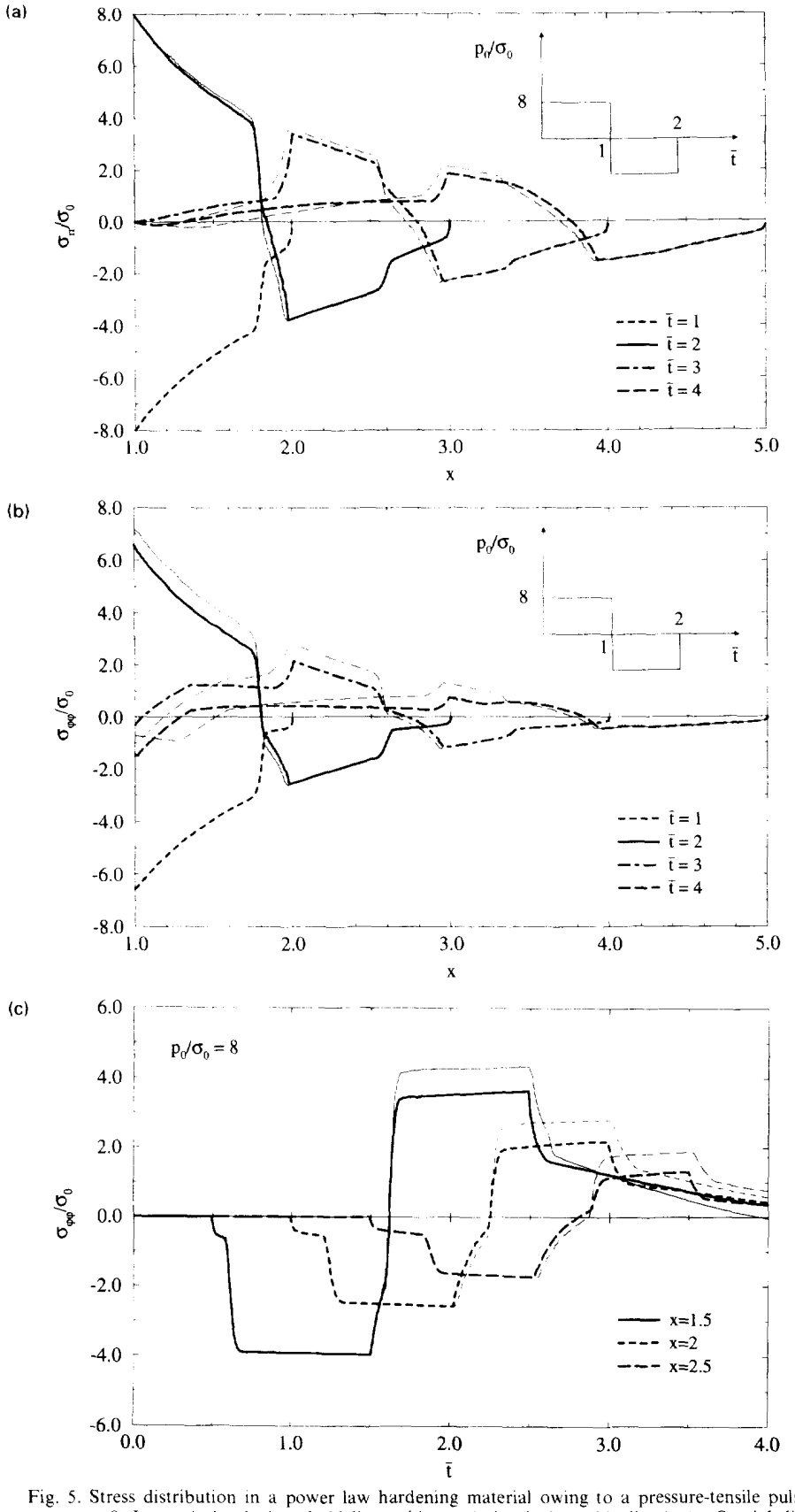

Fig. 5. Stress distribution in a power law hardening material owing to a pressure-tensile pulse $p_0/\sigma_0 = \pm 8$. Isotropic hardening (bold lines), kinematic hardening (thin lines). (a) Spatial distribution of the radial stress; (b) Spatial distribution of the circumferential stress; (c) Time variation of the circumferential stress.

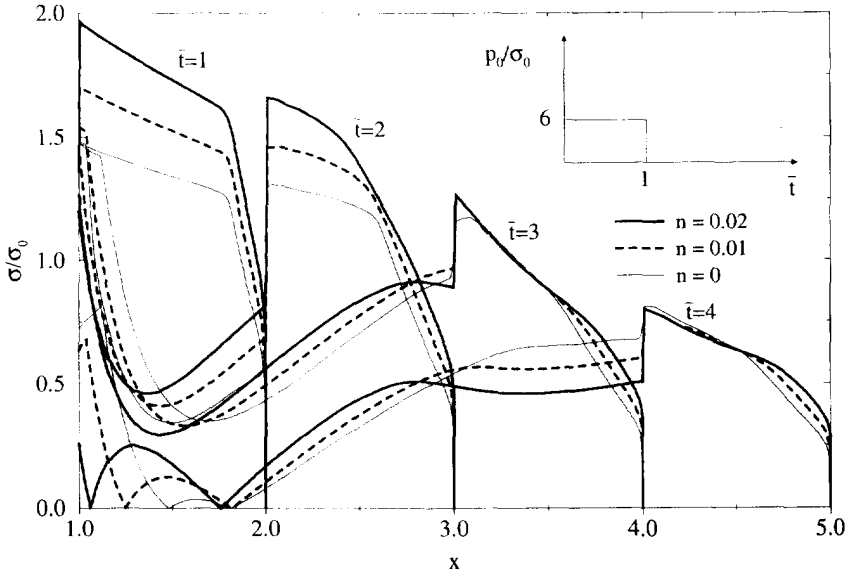

Fig. 6. Spatial distribution of the effective stress in a viscoplastic material with three different rate-sensitivities $n = 0, 0.01, 0.02$. Loading by a rectangular pressure pulse $p_0/\sigma_0 = 6$.

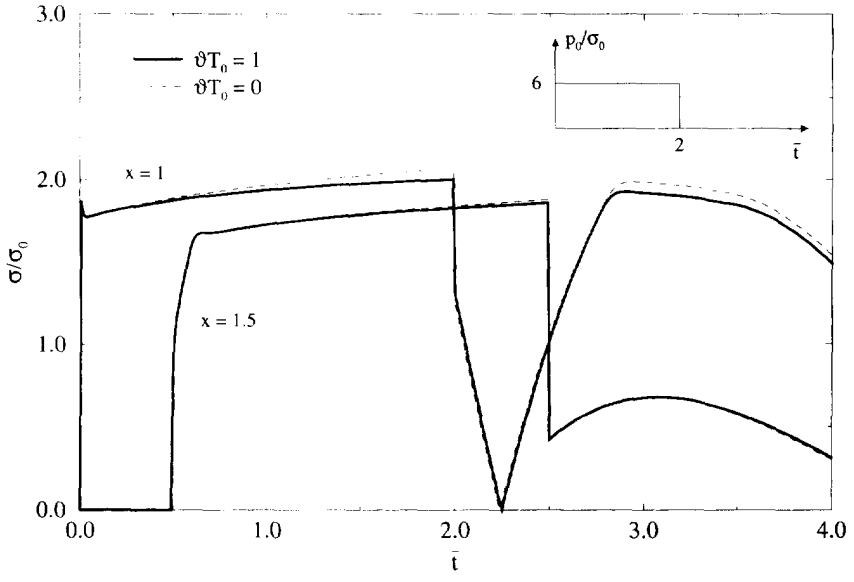

Fig. 7. Time variation of effective stress in a viscoplastic material, $n = 0.02$; $p_0/\sigma_0 = 6$. Thermal softening ($\vartheta T_0 = 1$) and no thermal softening ($\vartheta T_0 = 0$).

about $x = 3.5$. Finally, Fig. 9 shows the response for different values of the thermal expansion coefficient α. It is seen that a significant difference in the stresses appears only in the unloading domain behind the unloading wave front.

Acknowledgement—This work was supported through a grant by the Austrian National Science Foundation FWF under project P09533-TEC.

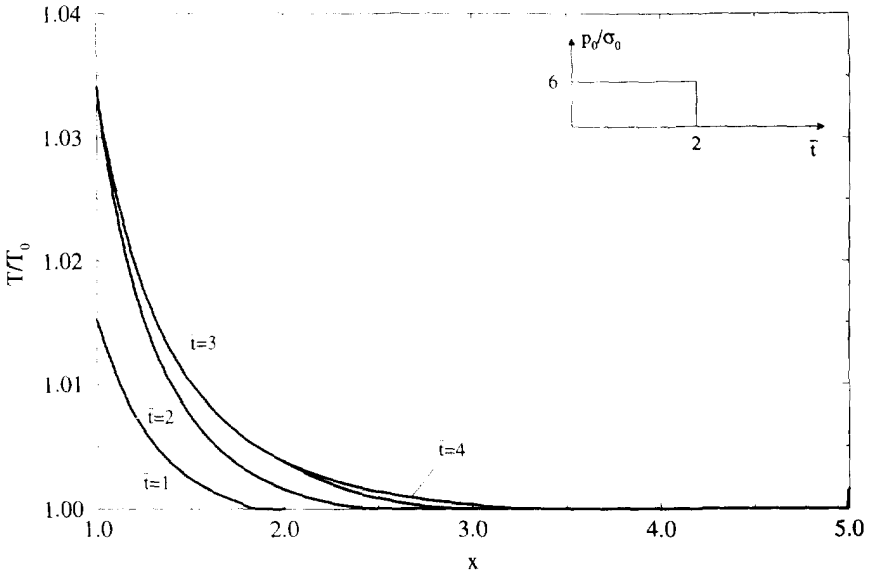

Fig. 8. Temperature distribution in a viscoplastic material, $n = 0.02$; $p_0/\sigma_0 = 6$.

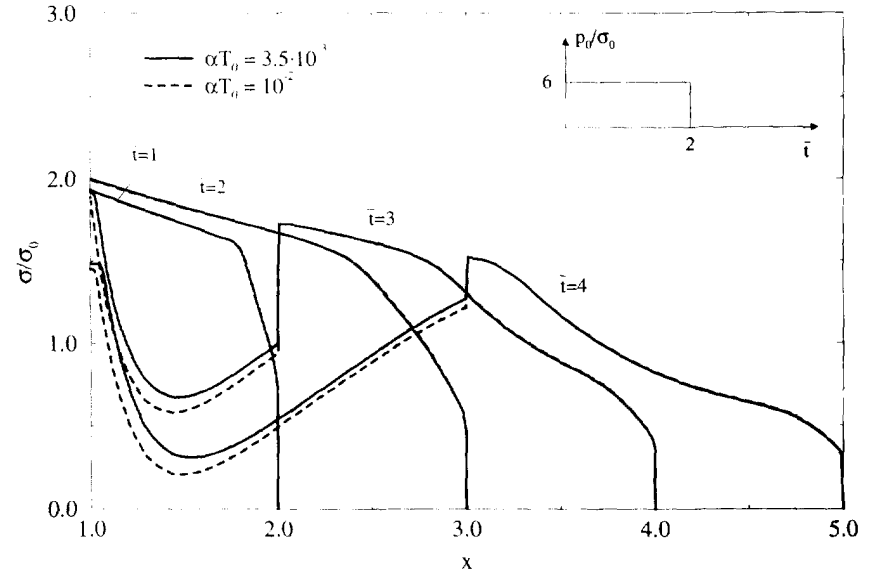

Fig. 9. Spatial distribution of the effective stress in a viscoplastic material $n = 0.02$; $p_0/\sigma_0 = 6$. Response for different values of the expansion coefficient α.

REFERENCES

Banerjee, P. K. (1994). *The Boundary Element Methods in Engineering*. McGraw-Hill, London.

Bodner, S. R. and Aboudi, J. (1983). Stress wave propagation in rods of elastic-viscoplastic materials. *Int. J. Solids Structures* **19**, 305–314.

Chadwick, P. (1970). Spherical waves in elastic-plastic materials. In *Inelastic Behavior of Solids* (Edited by W. F. Adler *et al.*), pp. 447–469. McGraw-Hill, New York.

Chadwick, P. and Morland, L. W. (1969). The starting problem for spherical elastic-plastic waves of small amplitude. *J. Mech. Phys. Solids* **17**, 419–436.

Eringen, A. C. and Suhubi, E. S. (1975). *Elastodynamics*, Vol. II. Academic Press, New York.

Eshelby, J. D. (1957). The determination of the elastic field of an ellipsoidal inclusion, and related problems. *Proc. R. Soc. Lond.* **A241**, 376–396.

Fotiu, P. A. (1995). A modified generalized midpoint rule for the integration of rate-dependent thermo-elastic-plastic constitutive equations. *Comp. Meth. Appl. Mech. Engng* **122**, 105–129.

Graff, K. F. (1975). *Wave Motion in Elastic Solids*. Clarendon Press, Oxford.

Güldenpfennig, J. and Clifton, R. J. (1980). Plastic waves of combined stress based on self-consistent slip models. *J. Mech. Phys. Solids* **28,** 201–219.
Hopkins, H. G. (1960). Dynamic expansion of spherical cavities in metals. In *Progress in Solid Mechanics* (Edited by I. N. Sneddon and R. Hill), Vol. I, pp. 83–164. North-Holland, Amsterdam.
Hunter, S. C. (1957). The properties of spherically symmetric disturbances in ideally plastic materials. *Proc. Conf. Properties of Materials at High Rates of Strain*, p. 147. Institute of Mechanical Engineers, London.
Irschik, H. and Ziegler, F. (1990). Uniaxial dissipative elastic waves due to high velocity impact. Proc. IUTAM Symp. *Elastic Wave Propagation and Ultrasonic Nondestructive Evaluation* (Edited by J. D. Achenbach, S. K. Datta and Y. S. Rajapakse), pp. 333–338. North-Holland, Amsterdam.
Kolsky, H. (1963). *Stress Waves in Solids*. Dover, New York.
Lighthill, M. J. (1964). *Introduction to Fourier Analysis and Generalized Functions*. Cambridge University Press, Cambridge.
Milne, P. C., Morland, L. W. and Yeung, W. (1988). Spherical elastic-plastic wave solutions. *J. Mech. Phys. Solids* **36,** 15–28.
Mok, C. H. (1968). Dynamic expansion of a spherical cavity in an elastic, perfectly plastic material. *J. Appl. Mech.* **35,** 372–378.
Morland, L. W. (1969). Spherical wave propagation in elastic-plastic work-hardening solids. *J. Mech. Phys. Solids* **17,** 371–385.
Mura, T. (1987). *Micromechanics of Defects in Solids*, 2nd edn. Kluwer, Dordrecht.
Nemat-Nasser, S. and Hori, M. (1993). *Micromechanics: Overall Properties of Heterogeneous Materials*. North-Holland, Amsterdam.
Simo, J. C. and Taylor, R. L. (1985). Consistent tangent operators for rate-independent elastoplasticity. *Comp. Meth. Appl. Mech. Engng* **48,** 101–118.
Simo, J. C. and Taylor, R. L. (1986). A return mapping algorithm for plane stress elastoplasticity. *Int. J. Num. Meth. Engng* **22,** 649–670.
Timoshenko, S. and Goodier, J. N. (1970). *Theory of Elasticity*, 3rd ed. McGraw-Hill, New York.
Ziegler, F., Irschik, H. and Holl, H. (1995). Elastic-viscoplastic waves in a hollow sphere, Proc. IUTAM Symp. *Nonlinear Waves in Solids* (Edited by F. Norwood and J. L. Wegner), pp. 171–176. AMR, ASME, New York.

APPENDIX A

The solution of eqn (9) is most conveniently derived by introducing a displacement potential $\Phi(r, t)$, defined by

$$u = \Phi_{,r}. \tag{A1}$$

With (A1), we can rewrite (9) as follows

$$\left(\frac{1}{r}(r\Phi)_{,rr} - \frac{1}{c_1^2}\ddot{\Phi}\right)_{,r} = -\frac{\delta(t-\tau)\delta(r-r')}{4\pi r'^2(\lambda+2\mu)}. \tag{A2}$$

After integrating (A2) and setting $F(r, t) = r\Phi(r, t)$, we obtain a simple wave equation for F,

$$F_{,rr} - \frac{1}{c_1^2}\ddot{F} = -\frac{r}{4\pi r'^2(\lambda+2\mu)}\left[H(r-r')\delta(t-\tau) + \frac{c_1}{a}C(t)\right], \tag{A3}$$

where $C(t)$ is an arbitrary non-dimensional integration constant. A particular solution of (A3) is found by means of the Green's function $G(x-x', \bar{t}-\bar{\tau})$ of the scalar wave equation (Graff, 1975, p. 25)

$$\begin{aligned} F(x, x', \bar{t}-\bar{\tau}) &= -\frac{1}{4\pi x'^2(\lambda+2\mu)}\int_0^{\bar{t}}\int_0^{\hat{x}} G(x-\hat{x}, \bar{t}-\hat{\tau})\hat{x}[H(\hat{x}-x')\delta(\hat{\tau}-\tau) + C(\hat{\tau})]\,\mathrm{d}\hat{x}\,\mathrm{d}\hat{\tau} \\ &= \frac{c_1}{2\mu}\frac{\zeta H(\bar{t}-\bar{\tau})}{16\pi x'^2}\{4x[(\bar{t}-\bar{\tau})H(x-x'-(\bar{t}-\bar{\tau})) + \bar{C}(\bar{t})] + [(x+(\bar{t}-\bar{\tau}))^2 - x'^2] \\ &\quad \times [H(x-x'+(\bar{t}-\bar{\tau})) - H(x-x'-(\bar{t}-\bar{\tau}))]\}, \end{aligned} \tag{A4}$$

where

$$G(x-\hat{x}, \bar{t}-\hat{\tau}) = -\frac{c_1}{2}H(\bar{t}-\hat{\tau})[H(x-\hat{x}+(\bar{t}-\hat{\tau})) - H(x-\hat{x}-(\bar{t}-\hat{\tau}))] \tag{A5a}$$

$$\bar{C}(\bar{t}) = \int_0^{\bar{t}}(\bar{t}-\hat{\tau})C(\hat{\tau})\,\mathrm{d}\hat{\tau}, \tag{A5b}$$

and the non-dimensional variables x, x', $\bar{t}$, $\bar{\tau}$ and ζ are defined by (10a,b). The Green's function $\bar{u}'(x, x', \bar{t}-\bar{\tau})$ is then derived from

$$\bar{u}'(x, x', \bar{t}-\bar{\tau}) = \frac{1}{a^2}\left(\frac{F(x, x', \bar{t}-\bar{\tau})}{x}\right)_{,x}. \tag{A6}$$

which gives

$$\tilde{u}^r(x', x, \bar{t}-\bar{\tau}) = \frac{c_1}{2\mu a^2}\frac{\zeta H(\bar{t}-\bar{\tau})}{16\pi(xx')^2}(x^2+x'^2-(\bar{t}-\bar{\tau})^2)[H(x-x'+(\bar{t}-\bar{\tau}))-H(x-x'-(\bar{t}-\bar{\tau}))]. \tag{A7}$$

Furthermore, it can be shown that

$$H(\bar{t}-\bar{\tau})[H(x-x'+(\bar{t}-\bar{\tau}))-H(x-x'-(\bar{t}-\bar{\tau}))] = H(\bar{t}-|x-x'|-\bar{\tau}), \tag{A8}$$

which, when substituted into (A7), yields the result (12a).

The boundary conditions at the cavity are satisfied by adding to $\tilde{u}^r$ a proper homogeneous solution of (9), which we denote by $\tilde{u}_h$. Accordingly, the corresponding displacement potential F_h is a solution of the homogeneous wave equation $F_{h,rr}-\ddot{F}_h/c_1^2=0$. Hence, F_h can be represented by a D'Alembert solution $F_h(r,t)=f(t-(r-a)/c_1)$, where f describes the reflected outgoing wave, starting from the cavity with radius a. With f, the displacement $\tilde{u}_h$ is found as (Timoshenko and Goodier, 1970, p. 510)

$$\tilde{u}_h = -\frac{f}{r^2}-\frac{f'}{c_1 r}, \tag{A9}$$

where f' is the derivative of f with respect to its argument. The boundary condition at the cavity surface requires

$$\sigma_{rr}(r=a)=(\lambda+2\mu)(\tilde{u}^r_{,r}(r=a)+\tilde{u}_{h,r}(r=a))+2\lambda(\tilde{u}^r(r=a)+\tilde{u}_h(r=a))/a=0. \tag{A10}$$

Substituting $\tilde{u}^r$ and (A9) into (A10) results in a differential equation for $f(t)$.

$$f''(t)+2\zeta\frac{c_1}{a}f'(t)+2\zeta\left(\frac{c_1}{a}\right)^2 f(t)=q(t), \tag{A11}$$

with

$$q(t)=-\frac{c_1^2}{2\mu a^2}\frac{\zeta}{16\pi x^2}\{[2\zeta((\bar{t}-\bar{\tau})^2-x^2)+2(1-\zeta)]H(\bar{t}-\bar{\tau}-x+1)-((\bar{t}-\bar{\tau})^2-x'^2-1)\delta(\bar{t}-\bar{\tau}-x'+1)\}. \tag{A12}$$

Equation (A11) has the structure of the equation of motion of a damped single-degree-of-freedom oscillator, which can be solved by means of the corresponding dynamic Green's function

$$\check{f}(\bar{t}-\bar{\theta})=\frac{a}{c_1}\frac{H(\bar{t}-\bar{\theta})}{\omega}\exp(-\zeta(\bar{t}-\bar{\theta}))\sin(\omega(\bar{t}-\bar{\theta})). \tag{A13}$$

Since $q(t)$ vanishes for $t<\tau+(r-a)/c_1$, the solution of (A11) can be written as

$$f(\bar{t}',\bar{\tau})=\frac{a}{c_1}\int_0^{\bar{t}'}\check{f}(\bar{t}'-\bar{\theta})q(\bar{\theta}')\,\mathrm{d}\bar{\theta}', \tag{A14}$$

where the prime denotes a shifted time scale, for example, $\bar{t}'=\bar{t}-\bar{\tau}-x'+1$. For $r>a$, t has to be replaced by the D'Alembert argument $t-(r-a)/c_1$, or, in non-dimensional form, we substitute $\bar{t}-x+1$ for $\bar{t}$. Hence, we may introduce a non-dimensional time measure $\xi=\bar{t}-\bar{\tau}-x-x'+2$, and find $\tilde{u}^r=\tilde{u}_h$ from (A9) as

$$\tilde{u}^r(x,x',\bar{t}-\bar{\tau})=-\frac{1}{a}\left(\frac{f(\xi)}{x^2}+\frac{f'(\xi)}{x}\right). \tag{A15}$$

If the integration (A14) is carried out and the result is introduced into (A15), we obtain formula (12b) for the reflected wave $\tilde{u}^r$.

APPENDIX B

The Green's functions of the deviatoric strains ε^d_{ij} are derived from $\tilde{u}$ by proper differentiation. In particular, we have

$$\tilde{e}=\tfrac{1}{2}(\tilde{u}_{,r}-\tilde{u}\,r), \quad \tilde{s}=\tfrac{1}{2}(\tilde{\sigma}_{,r}-\tilde{\sigma}\,r), \quad \tilde{s}_m=\tfrac{1}{2}(\tilde{\sigma}_{m,r}-\tilde{\sigma}_m r). \tag{B1}$$

The individual incident and reflected components are:

(1) $\underline{\dot{\tilde{e}}}, \underline{\tilde{e}}$:

$$\tilde{e}^{I}(x', x, \bar{t}-\bar{\tau}) = \tilde{\sigma}^{I}(x, x', \bar{t}-\bar{\tau})/3\mu, \quad \tilde{e}^{r}(x', x, \bar{t}-\bar{\tau}) = \tilde{\sigma}^{r}(x, x', \bar{t}-\bar{\tau})/3\mu, \tag{B2a}$$

$$\tilde{e}(1, x, \bar{t}-\bar{\tau}) = -\frac{c_1}{2\mu a^4}\frac{\zeta}{6\pi x^3}\left\{\left[\frac{H(\xi)\exp(-\zeta\xi)}{\omega}\cdot[(3(1-\zeta x)-2\zeta x^2(1-\zeta))\sin(\omega\xi) + \omega x(3-2\zeta x)\cos(\omega\xi)] + x^2\delta(\xi)\right\}, \tag{B2b}$$

$$\dot{\tilde{e}}^{I}(x', x, \bar{t}-\bar{\tau}) = \frac{c_1^2}{2\mu a^4}\frac{\zeta}{12\pi x^3 x'^2}[3(\bar{t}-\bar{\tau})H(\bar{t}-d-\bar{\tau}) + 2x(x-2x')\delta(\bar{t}-d-\bar{\tau}) - \frac{x}{2}(x^2+x'^2-(\bar{t}-\bar{\tau})^2)\operatorname{sgn}(x-x')\delta'(\bar{t}-d-\bar{\tau})], \tag{B3a}$$

$$\dot{\tilde{e}}^{r}(x', x, \bar{t}-\bar{\tau}) = -\frac{c_1^2}{2\mu a^4}\frac{\zeta}{12\pi x^3 x'^2}\left\{\left[3(\xi+\bar{x}-1) - \frac{2\exp(-\zeta\xi)}{\omega}\cdot[\zeta\{3(1-2\zeta xx'+2\bar{x}) - 2\zeta x^2(1+2x'(1-\zeta))\}\sin(\omega\xi) - \omega\{3(1-2\zeta xx') - 2\zeta x^2(1-2\zeta x')\}\cdot\cos(\omega\xi)]\right]H(\xi) + 2x(x+2x'-4\zeta xx')\delta(\xi) + \frac{x}{2}\mathscr{H}(x', x, \bar{t}-\bar{\tau})\delta'(\xi)\right\}. \tag{B3b}$$

(2) $\underline{\tilde{s}, \tilde{s}_m}$:

$$\tilde{s}^{I}(x', x, \bar{t}-\bar{\tau}) = -\frac{c_1}{a^4}\frac{\zeta}{24\pi(xx')^3}[3(3(\bar{t}-\bar{\tau})^2 - x^2 - x'^2)H(\bar{t}-d-\bar{\tau}) - 8xx'd\delta(\bar{t}-d-\bar{\tau}) + xx'(x^2+x'^2-(\bar{t}-\bar{\tau})^2)\delta'(\bar{t}-d-\bar{\tau}) - 4(xx')^2\delta(x-x')\delta(\bar{t}-\bar{\tau})], \tag{B4a}$$

$$\tilde{s}^{r}(x', x, \bar{t}-\bar{\tau}) = \frac{c_1}{a^4}\frac{\zeta}{24\pi(xx')^3}\left\{\left[9\mathscr{H}(x', x, \bar{t}-\bar{\tau}) + 6(x^2+x'^2) - 8\zeta\frac{\exp(-\zeta\xi)}{\omega}\cdot[\{3(x^2+x'^2) - \zeta xx'(3(x+x') + 2(1-\zeta)xx')\}\sin(\omega\xi) + \omega(3(x+x') - 2\zeta xx')xx'\cos(\omega\xi)]\right]H(\xi) + 8xx'(1+\bar{x}-2\zeta xx')\delta(\xi) + xx'\mathscr{H}(x', x, \bar{t}-\bar{\tau})\delta'(\xi)\right\}, \tag{B4b}$$

$$\tilde{s}^{I}_{m}(x', x, \bar{t}-\bar{\tau}) = -\frac{c_1}{a^4}\frac{3-2\zeta}{36\pi x^3 x'^2}[3x'H(\bar{t}-d-\bar{\tau}) + (4x'-x)x\operatorname{sgn}(x-x')\delta(\bar{t}-d-\bar{\tau}) + \frac{x}{2}(x^2+x'^2-(\bar{t}-\bar{\tau})^2)\delta'(\bar{t}-d-\bar{\tau}) - 2x^2x'\delta(x-x')\delta(\bar{t}-\bar{\tau})], \tag{B5a}$$

$$\tilde{s}^{r}_{m}(x', x, \bar{t}-\bar{\tau}) = \frac{c_1}{a^4}\frac{3-2\zeta}{36\pi x^3 x'^2}\left\{\left[3x' - \frac{4\zeta x'\exp(-\zeta\xi)}{\omega}\cdot[(3-3\zeta x-2\zeta(1-\zeta)x^2)\sin(\omega\xi) + \omega(3-2\zeta x)x\cos(\omega\xi)]\right]H(\xi) + x(4x'+x-8\zeta xx')\delta(\xi) + \frac{x}{2}\mathscr{H}(x', x, \bar{t}-\bar{\tau})\delta'(\xi)\right\}. \tag{B5b}$$

(3) $\underline{\dot{\tilde{\sigma}}, \dot{\tilde{\sigma}}_m, \ddot{\tilde{u}}}$:

$$\dot{\tilde{\sigma}}^{I}(x', x, \bar{t}-\bar{\tau}) = 3\mu\dot{\tilde{e}}^{I}(x, x', \bar{t}-\bar{\tau}), \quad \dot{\tilde{\sigma}}^{r}(x', x, \bar{t}-\bar{\tau}) = 3\mu\dot{\tilde{e}}^{r}(x, x', \bar{t}-\bar{\tau}), \tag{B6}$$

$$\dot{\tilde{\sigma}}^{I}_{m}(x', x, \bar{t}-\bar{\tau}) = \frac{c_1^2}{2\mu a^4}\frac{3-2\zeta}{24\pi x^2 x'^3}[x'(2x'-x)\delta(\bar{t}-d-\bar{\tau}) + \frac{x'}{2}(x^2+x'^2-(\bar{t}-\bar{\tau})^2)\operatorname{sgn}(x-x')\delta'(\bar{t}-d-\bar{\tau})], \tag{B7a}$$

$$\dot{\tilde{\sigma}}^{r}_{m}(x', x, \bar{t}-\bar{\tau}) = -\frac{c_1^2}{2\mu a^4}\frac{\zeta}{24\pi x^2 x'^3}\left\{4\zeta x'^2H(\zeta)\frac{\exp(-\zeta\xi)}{\omega}\cdot[\zeta(1+2(1-\zeta)x)\sin(\omega\xi) - \omega(1-2\zeta x')\cos(\omega\xi)] + x'(2x'+x-8\zeta xx')\delta(\xi) + \frac{x'}{2}\mathscr{H}(x', x, \bar{t}-\bar{\tau})\delta'(\xi)\right\}. \tag{B7b}$$

$$\ddot{u}^r(x', x, \bar{t}-\bar{\tau}) = -\frac{c_1^2}{2\mu a^4}\frac{\zeta}{8\pi(xx')^2}[H(\bar{t}-d-\bar{\tau}) + 2d\delta(\bar{t}-d-\bar{\tau}) - \tfrac{1}{2}(x^2+x'^2-(\bar{t}-\bar{\tau})^2)\delta'(\bar{t}-d-\bar{\tau})], \quad \text{(B8a)}$$

$$\ddot{u}^r(x', x, \bar{t}-\bar{\tau}) = \frac{c_1^2}{2\mu a^4}\frac{\zeta}{8\pi(xx')^2}\left\{\left[1-\frac{4\zeta\exp(-\zeta\xi)}{\omega}\right.\right.$$
$$\left.\cdot[\tfrac{1}{4}(1-\zeta)(1-2\zeta xx')-\zeta\bar{x}_1^2\sin(\omega\xi)+\omega\tfrac{1}{4}(1-2\zeta xx'+\bar{x}_1^2\cos(\omega\xi)]\right]H(\xi)$$
$$\left.+2(\bar{x}+1-4\zeta xx')\delta(\xi)+\tfrac{1}{2}\mathscr{U}(x', x, \bar{t}-\bar{\tau})\delta'(\xi)\right\}. \quad \text{(B8b)}$$

In the above equations, δ' denotes the derivative of the delta function with respect to its argument. This function is defined by (Lighthill, 1964)

$$\int_a^b f(x)\delta'(x-\xi)\,\mathrm{d}x = -f'(\xi)[H(\xi-a)-H(\xi-b)], \quad \delta'(x-\xi) = -\delta'(\xi-x). \quad \text{(B9)}$$

In (B4a) and (B5a) we also made use of the relation

$$\frac{\mathrm{d}}{\mathrm{d}x}\operatorname{sgn}(x-x') = 2\delta(x-x'). \quad \text{(B10)}$$